Simulation of equinus gait and effects of ankle stiffness compensation with a neuromusculoskeletal model

Francesca Santini

Master of Science Thesis

TU Delft Delft University of Technology

Simulation of equinus gait and effects of ankle stiffness compensation with a neuromusculoskeletal model

Master Thesis

in partial fulfilment of the requirements for the degree of

Master of Science
in Biomedical Engineering

at Delft University of Technology,
to be defended on Friday October 30th, 2020 at 11:00 a.m.

by

Francesca Santini

Thesis committee:

Dr. Ir. M. Mirzaali Mazandarani	TU Delft
Dr. Ir. L. Peternel	TU Delft
Dr. Ir. W. Mugge	TU Delft
Dr. Ir. A. C. Schouten	TU Delft
Dr. Ir. J.H. de Groot	LUMC
Dr. M. Stijntjes	LUMC
Ir. K. E. Rodriguez	TU Delft

Abstract

Introduction: Pes equinus with increased ankle joint stiffness is a common impairment in stroke and Cerebral Palsy (CP) patients with structural and/or neural deficits of the ankle muscles. Equinus gait is characterized by toe-strike, abnormal ankle plantarflexion and decreased ankle range of motion (ROM). A new ankle-foot orthosis (AFO) with negative stiffness was previously developed to compensate for the increased ankle joint stiffness and improve equinus gait, reducing plantarflexion and increasing ankle ROM. The goal of this project was to predict the effects of ankle stiffness compensation on equinus gait simulations.

Methods: Forward simulations of unimpaired and equinus gait were generated in the sagittal plane with a musculoskeletal model implemented in OpenSim and a neural controller implemented in SCONE. After validation of the unimpaired gait simulation, a sensitivity analysis on ankle kinematics was performed, introducing structural and/or neural alterations of the ankle muscles to achieve an equinus gait. Consecutively, equinus gait simulations were validated with previously collected data of CP patients. Finally, an AFO model was developed in OpenSim to simulate AFO-assisted gait.

Results: The unimpaired gait simulation yielded realistic results, and was robust to all alterations, generating stable gaits. Shorter Gastrocnemius fiber length and/or increased plantarflexor muscles activations, with Tibialis Anterior weakness, had the largest effect on the ankle joint kinematics and resulted in realistic CP equinus gaits. Simulations of AFO-assisted gait resulted in reduced abnormal plantarflexion, and increased ankle ROM in the condition with shorter Gastrocnemius.

Discussion and Conclusion: This study presented realistic simulations of equinus gait, by modelling structural and/or neural alterations of the ankle muscles and predicted improved ankle function when compensating ankle stiffness with an external force. Although higher stiffness compensation and more simulations should be obtained, this study provides a solid ground for further investigation of the AFO effects. These results can ultimately assist in the prescription and tuning of the new AFO for patients with equinus.

Contents

List of abbreviations

AFO	Ankle-Foot Orthosis
CMA-ES	Covariance Matrix Adaptation-Evolution Strategy
COM	Center Of Mass
CP	Cerebral Palsy
DF	Dorsiflexion (rotation of the ankle so that foot points up)
DOF	Degree Of Freedom
EMG	Electromyography
FB	Feedback
HAM	Hamstrings
ILP	Iliopsoas
GAS	Gastrocnemius (Medialis and Lateralis)
GM	Gluteus Maximus
GRF	Ground Reaction Force
NCC	Normalized Cross Correlation
NMS	Neuromusculoskeletal
PF	Plantarflexion (rotation of the ankle so that foot points down)
RMSE	Root-Mean-Squared Error
ROM	Range Of Motion
SD	Standard Deviation
SOL	Soleus
TA	Tibialis Anterior
VAS	Vasti (Medialis and Lateralis)

1

Introduction

1.1. Background

Equinus gait, or toe-walking, is observed in 10-20% of stroke patients, and most of the patients with Cerebral Palsy (CP) [1–3]. Equinus gait is characterized by initial foot contact occurring with the toes, abnormal plantarflexion of the ankle, and restricted ankle active range of motion (ROM) [4, 5]. Patients with equinus develop ways to compensate for their limited ankle motion with increased hip and knee flexion, or knee hyperextension, resulting in slower walking velocity, increased metabolic cost, instability and pain [5]. Equinus deformity of the foot often occurs unilaterally [2], and is associated with muscle weakness [6] and increased passive stiffness of the ankle joint (i.e. increased resistance to movement in response to a passive stretch). Increased stiffness results from a combination of neural and structural deficits of the ankle muscles: spasticity, improper muscle activation, hyperreflexia, muscle contractures, shorter muscle fibers, fewer fibers and higher collagen concentration in the extracellular matrix [7, 8].

Ankle-foot orthoses (AFOs) are assistive devices prescribed with the aim of improving gait function of patients with equinus [9]. The most common AFOs are passive (non-actuated) devices, which counteract equinus by fixing the foot in a position perpendicular to the shank [10]. However, passive AFOs increase the stiffness of the combined Ankle+AFO system, restricting the dorsiflexion and plantarflexion movements. To solve this problem, a new AFO with negative stiffness has been developed by Rodriguez et al., 2018 [11] to compensate, instead of increase, the excessive passive ankle joint stiffness. The main target population of the AFO are chronic stroke patients and CP patients with equinus. The new AFO does not restrict ankle movements in the sagittal plane, allowing for a ROM of 20 degrees in dorsiflexion and 60 degrees in plantarflexion, wider than the ROM required for everyday activities [12]. The mechanism of the new AFO exerts a torque in function of the ankle rotation, adjustable to compensate for the ankle joint stiffness of multiple patients. The main function of the new AFO is to support the Tibialis Anterior (TA) muscle to clear

the foot during the swing phase and to control the rotation of the ankle during the stance phase. A first wearable prototype has been developed (Fig. 1.1), however, due to COVID-19 restrictions, it has not yet been tested on a clinical population of stroke patients with equinus.

Figure 1.1: The new ankle-foot orthosis with negative stiffness has an L-shaped carbon frame around the foot and ankle. The foot part can be fitted inside a shoe. The hinge is placed laterally and close to the ankle joint.

Forward simulations with neuromusculoskeletal (NMS) models are a tool to investigate the influence on gait kinematics of perturbations, such as muscular and/or neural deficits and AFOs for rehabilitation. NMS models simulate movements produced by the muscular and skeletal systems controlled by the nervous system [13]. Forward simulations use as input neural commands, either from experimental electromyographic (EMG) muscle activity, or from a neural model (i.e., controller), and compute motion trajectories that perform a given task (walking, jumping, running, etc.), optimizing objectives such as stability, energy efficiency and pain avoidance. Forward simulations are still on the state of the art research and not broadly used, because choice of the optimization criteria is questionable, optimizations are time consuming, and it is difficult to reproduce previous work, due to the sensitivity of the simulation to a software environment and limited sharing of software and models. Moreover, the prediction of the interaction between NMS and orthosis models is not straightforward, given the limited understanding of the influence of AFO characteristics on muscle function during gait [14].

Previous studies investigated the effects of muscular structural and/or neural deficits and AFOs on forward simulations, however none of them considered both structural and neural deficits commonly seen in pathological populations and their combinations, and not all of them simulated gait. A study by Ong et al. 2019 [15] used a musculoskeletal model and a reflex-based controller to generate simulations of normal gait and equinus gait in the sagittal plane, but only investigated the effects of decreased optimal length and reduced maximum force of the plantarflexor muscles independently. Higginson et al. 2006 [16] simulated equinus gait increasing ankle plantarflexion angle at initial contact during a forward simulation of healthy gait, without introducing any structural or neural alterations of the musculoskeletal model. Luengas et al. 2015 [17] simulated hemiparetic gait increasing stiffness of the modelled impaired limb, without considering other muscular structural or neural

deficits. Spasticity has been modelled with increased feedback from muscle velocity, length, acceleration, force and its time derivative [18–21]. The limitation of all of these models is that they were not applied during gait, but during passive muscle stretches, except the study of Jansen et al. 2014 [20], that however did not consider altered muscle structural properties. AFO models have been combined with healthy musculoskeletal models and forward simulations of healthy gait to explore the influence of AFOs on joint moments and muscle excitations [14, 22]. The limitation of these studies is that they use healthy models, and therefore they do not assess the effects of AFOs on pathological gait patterns. Rosenberg et al. 2017 [23] simulated the impact of AFOs on muscle demand and recruitment in children with CP and crouch gait, however they assumed identical kinematics between no-AFO and AFO conditions, therefore, the effect of AFO on kinematics of crouch gait could not be assessed.

1.2. Goal and approach

The goal of this study is to generate simulations of the equinus gait by using a NMS model that includes both muscular and neural alterations contributing to increased ankle joint stiffness, and predict the effects of ankle stiffness compensation on the equinus gait with a model of the new AFO. To achieve the goal of the study, a step-wise approach is followed (Fig. 1.2). The first step is to generate and validate a forward simulation of unimpaired gait in the sagittal plane with a two-dimensional musculoskeletal model implemented in OpenSim [24, 25] and a neural controller implemented in SCONE [26]. The second step is to generate and validate forward simulations of equinus gait by performing a sensitivity analysis of structural and neural alterations of the muscles around the ankle joint associated with equinus. The third step is to generate predictive simulations of AFO-assisted equinus gait, by developing a model of the new AFO with negative stiffness.

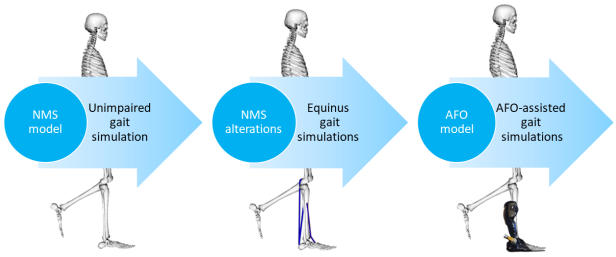

Figure 1.2: Step-wise approach. Firstly, a forward simulation of unimpaired gait is generated by using a neuromusculoskeletal (NMS) model. Secondly, structural and neural alterations of the muscles around the ankle joint are introduced in the NMS model and simulations of the equinus gait are generated. Thirdly, a model of the ankle foot orthosis (AFO) is developed and AFO-assisted gait simulations are generated.

2

Methods

2.1. Neuromusculoskeletal model

To generate unimpaired and equinus gait simulations in the sagittal plane, the musculoskeletal model was implemented in OpenSim 3.3 [24, 25], and the optimization and neural gait controller was implemented in SCONE 1.5 [26]. The musculoskeletal model included 9 degrees of freedom (DOF) and 14 muscles (Fig. 2.1).
The gait controller, based on Geyer et al. 2010 [27], computed muscle excitations over time, based on feedback (FB) from muscle length and velocity, muscle force, and joint angles, with the addition of a time shift to simulate neural delays (Eq. 2.1), modelling proprioceptive FB from muscle spindles (muscle length and velocity), Golgi tendon organs (muscle force) and joint receptors (joint movement).

$$u(t) = C_0 + K_L[l(t - t_D) - l_0] + K_V[v(t - t_D) - v_0] + K_F[F(t - t_D) - F_0] + K_P[P(t - t_d) - P_0] \tag{2.1}$$

$u(t)$	muscle excitation	v_0	velocity FB offset
C_0	constant excitation	K_F	force FB gain
K_L	length FB gain	F	muscle force
l	muscle length	F_0	force FB offset
t_D	time shift	K_P	joint angle FB gain
l_0	length FB offset	P	joint angle
K_V	velocity FB gain	P_0	joint angle offset
v	muscle velocity		

Muscle activations were computed from muscle excitations using a first-order dynamic model and muscle forces were computed from muscle activations using a Hill-type muscle contraction dynamics model. Hill-type muscles produced active force up to a maximum value depending on fiber length, velocity and activation,

and passive force, depending on fiber length. The total force was the sum of the active and passive forces (Fig. 2.4a).

To generate a gait simulation, a dynamic optimization problem was solved (Fig. 2.2). The goal of the optimizer was to find the controller parameters (reflex gains and offsets, Eq. 2.1) that minimize the objective function, and it was based on a covariance matrix adaptation evolution strategy (CMA-ES) algorithm. The objective function represented the task to be performed (walking) and was defined as a weighted combination of measures: maximize speed, minimize energy consumption, prevent knee and ankle hyperextension. Additional measures limiting vertical ground reaction forces (GRF), ankle velocity, hip displacement, stride duration and length were implemented in the objective function (Appendix 5) to generate more realistic results at the ankle joint.

2.2. Unimpaired gait simulation

The simulation of the unimpaired gait was validated with a data set of 20 healthy subjects walking overground at self-selected speed from Bovi et al., 2011 [28]. Outputs of the SCONE simulations and OpenSim Inverse Dynamics Tool - sagittal plane hip, knee and ankle joints angles, ankle and knee moments normalized per body mass, and vertical GRF - were compared with experimental data over the gait cycle (defined from right heel strike to consecutive right heel strike, Fig. 2.3)

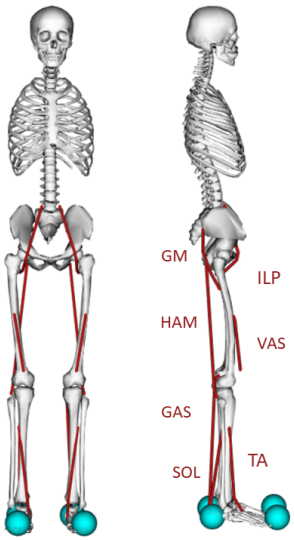

Figure 2.1: Planar musculoskeletal model used for gait simulations. The model included 14 muscles, 7 per leg: Gluteus Maximus (GM), Iliopsoas (ILP), Hamstrings (HAM), Vasti (VAS), Gastrocnemius Medialis and Lateralis (GAS), Tibialis Anterior (TA), Soleus (SOL). The model had 9 degrees of freedom: 3 at the pelvis and one at each hip, knee and ankle. The blue spheres comprised the compliant contact model used to generate forces between the feet and the ground.

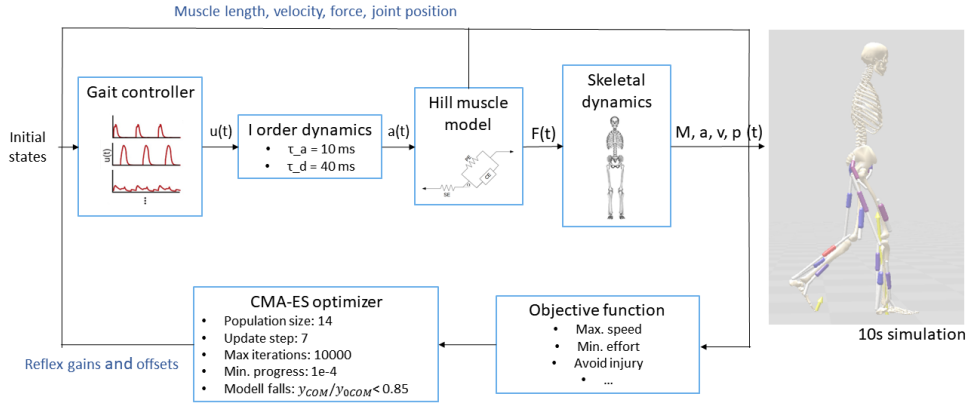

Figure 2.2: Shooting-based approach used for the forward simulation of motion. The simulation was performed multiple times, and starting from an initial set of parameters for the first iteration, the gait controller updated muscle excitations $u(t)$ at each iteration, based on sensory feedback (from muscle length, velocity, force, joint position) and optimized reflex gains and offsets. The first-order dynamic model computed muscle activations $a(t)$, with activation (τ_a) and deactivation (τ_d) time constants of 10 ms and 40 ms, respectively. The Hill-type muscle contraction dynamics model computed muscle forces $F(t)$ based on muscle activation, muscle length and velocity. Skeletal dynamics and integration of the equations of motion transformed muscle forces to joint moments $M(t)$ and movements of the skeletal segments (accelerations $a(t)$, velocities $v(t)$ and positions $p(t)$). The simulation time was set to 10 seconds. The objective function quantified the performance of each simulation based on a weighted sum of measures. The goal of the optimizer was to find the parameters for which the objective function was minimized. At each iteration, 14 new solutions were generated by variation of the previous solutions. At each update step, 7 solutions were selected, based on their fitness value from the objective function. The optimization ran for a maximum number of iterations, or until the objective function stopped improving significantly (min. progress). The optimization terminated earlier if the center of mass (COM) was below a certain threshold, meaning that the model fell down.

in terms of root-mean-squared error (RMSE) reported in units of standard deviation (SD), and normalized cross correlation (NCC). RMSE measured the difference between simulated and experimental mean values, NCC measured shape similarity between the simulated and experimental data sets on a scale from 0 to 1 [29]. If the RMSE was lower than 2 SD and the NCC was higher than 0.5, it meant the model could capture experimental trends, both in values and shapes, and therefore used in the following steps with the equinus gait simulations. Simulated muscle activations were compared to on-off timings of EMG reported by Perry et al., 1992 [30], to identify when muscles were active.

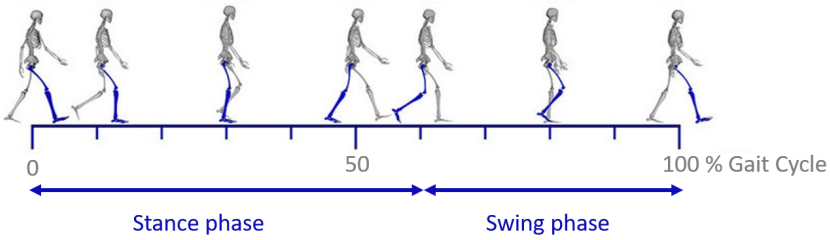

Figure 2.3: Gait cycle, defined from right heel strike to consecutive right heel strike. During the Stance Phase, the right foot remained in contact with the ground, while during the Swing Phase, it remained lifted.

2.3. Equinus gait simulations

2.3.1. NMS model alterations

After the validation of the unimpaired gait, alterations to be introduced in the NMS model were identified by a literature search on neural and muscular structural deficits reported after stroke and CP. The complete list of alterations is provided in Appendix 5, and the final 15 selected alterations are presented in Table 2.1. Three simulations with combinations of alterations were also performed, for a total of 18 simulations. All alterations were applied on the right side of the body and the neural controller generated asymmetric commands for right and left muscles.

Table 2.1: Isolated alterations introduced in the Neuromusculoskeletal (NMS) model, in the muscles around the right ankle joint - Tibialis Anterior (TA), Gastrocnemius (GAS) or Soleus (SOL) - associated with structural and neural deficits of stroke or Cerebral Palsy patients.

NMS model alterations	Deficits in patients	Ref.
↓ TA max isometric force	Dorsiflexor muscles weakness	[31–34]
↓ GAS, SOL optimal fiber length	Plantarflexor muscles shortening	[15, 35–38]
↑ GAS, SOL passive stiffness	Plantarflexor muscle stiffness	[37, 39]
↓ GAS, SOL max isometric force	Plantarflexor muscles weakness	[15, 36, 40, 41]
↑ GAS, SOL min activation	Plantarflexor muscles overactivity	[42–45]
↑ GAS, SOL velocity FB	Reflex hyper-excitability	[18, 19, 42, 46]
↑ GAS, SOL velocity and length FB		[20, 21, 46]
↑ GAS, SOL force FB		[21, 46, 47]

Dorsiflexor muscle weakness was simulated decreasing the maximum isometric force that the TA muscle of the model can generate (Fig. 2.4b). Shorter GAS and SOL fascicle length due to reduced number of sarcomeres in series and/or shorter sarcomeres were simulated decreasing the optimal fiber length of the GAS and SOL (Fig. 2.4c), as in Ong et al. 2019 [15]. Increased passive stiffness of the plantarflexor muscles was simulated increasing the slope of the passive force-length curve of GAS and SOL, decreasing fiber strain at which maximum force was generated (Fig. 2.4d).

Plantarflexor muscle weakness was simulated decreasing the maximum isometric force of the GAS and SOL muscles, as in Ong et al. 2019 [15]. Increased muscle tone and overactivity of spastic plantarflexor muscles was simulated increasing the minimum activation level of GAS and SOL. Reflex hyper-excitability of spastic muscles was simulated increasing reflexes based on feedback from muscle velocity, velocity and length, or muscle force, as previously developed models of spasticity [18–21], adding velocity (K_V), length (K_L) or force (K_F) feedback gains when computing the excitation of the SOL and GAS muscles with Eq. 2.1. A time delay of 20 ms was added to simulate the delay between the stretch of the muscle spindle and the generation of force in the muscle [18, 19, 21]. Combinations of dorsiflexor muscle weakness and/or shortening and/or overactivity of the triceps surae were simulated combining decreased TA maximum force, and/or decreased GAS and SOL optimal fiber length and/or increased GAS and SOL activation.

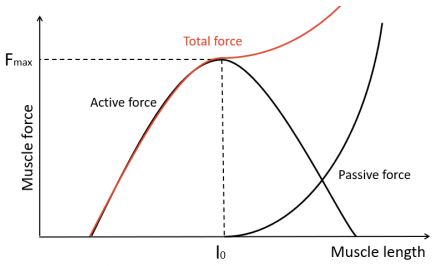

(a) Force-length curves of the unimpaired muscle.

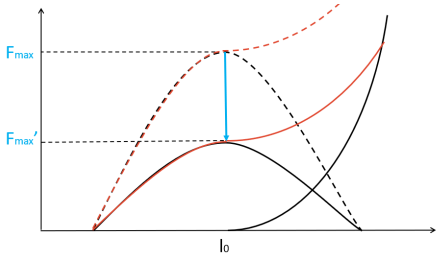

(b) Muscle paresis was simulated by a decreased maximum isometric force (F_{max}) that the muscle actively generated.

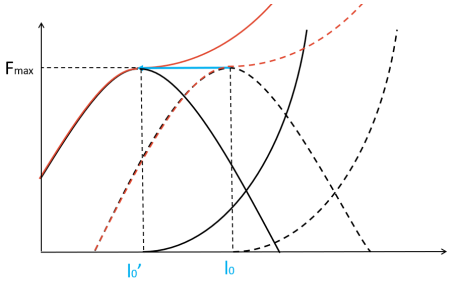

(c) Muscle shortening was simulated by a decreased optimal fiber length (l_0) of the muscle.

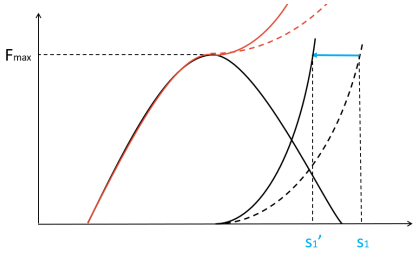

(d) Increased muscle passive stiffness - decreased passive fiber strain (s_1) at F_{max}.

Figure 2.4: The force that a muscle generates depended on active and passive properties, according to the Hill-type muscle model. Structural aspects of the increased ankle stiffness were simulated by altering active or passive force-length curves of the muscles around the ankle joint.

2.3.2. Sensitivity analysis

To provide insight into the relative contribution of different NMS alterations on simulated gait, a sensitivity analysis was performed. Sensitivity analysis is the study of how the uncertainty in the output (i.e. ankle angle during gait) of a model (i.e. NMS model) can be apportioned to different sources of uncertainty in the model inputs (i.e. alterations Table 2.1, inputs of the neural or muscle model) [48]. Selected alterations were gradually and systematically introduced in the NMS model (Tables 2.2), using the solutions of the previous simulations as the initial guesses for the following simulations, to speed up model convergence. Alterations were increased until the maximum or minimum value allowed in the model or until the model was not able to perform a 10 s simulation of gait without falling. Alterations selected for the combinations were also gradually combined, until the model was able to perform a 10 s simulation of gait without falling, and the maximum values were applied (Table. 2.3). The primary outcomes of the sensitivity analysis of equinus gait simulation were right ankle angles: trajectories were analysed during the simulated gait cycle, with each NMS model alteration at its maximum level. Simulations resulting in increased ankle plantarflexion and toe strike (equinus gait simulations) and toe-strike were selected for the analysis of the secondary outcomes: right hip and knee angles and ankle moments.

Table 2.2: Isolated alterations from the default value of the unimpaired model. Increase (↑) or decrease (↓) by equal-sized steps. The results of the previous simulation were used as the the initial guess for the following simulation, until the maximum alteration allowed, or until the model was not able to perform a 10 s simulation of gait without falling. F_{max} = maximum isometric force; l_0 = optimal fiber length; s_1 = passive strain; a_{min} = minimum activation; K_V, K_L, K_F velocity, length, force reflex gains (Eq. 2.1).

	Default	Step	Max/Min
↓ TA F_{max}	3000 N	150 N	1050 N
↓ GAS l_0	0.09 m	0.009 m	0.045 m
↓ SOL l_0	0.05 m	0.005	0.04 m
↓ SOL s_1	0.7	0.1	0.05
↓ GAS s_1	0.7	0.05	0.05
↓ GAS F_{max}	2500 N	250 N	0 N
↓ SOL F_{max}	5137 N	1027 N	0 N
↑ GAS a_{min}	0.01	0.01	0.2
↑ SOL a_{min}	0.01	0.01	0.6
↑ GAS K_V	0	0.1	1
↑ SOL K_V	0	0.1	1
↑ GAS K_V, K_L	0	0.1	1
↑ SOL K_V, K_L	0	0.1	1
↑ GAS K_F	1.1 (stance)	0.1	1
↑ SOL K_F	1.2 (stance)	0.1	1

Table 2.3: Combined alterations introduced in the model: decreased maximum isometric force (F_{max}) of the Tibialis Anterior (TA), and/or decrease optimal fiber length (l_0) of Gastrocnemius (GAS) and Soleus (SOL), and/or increased minimum activations (a_{min}) of GAS and SOL.

Combinations				
TA weakness	Plantarflexors shortening		Plantarflexors overactivity	
-10% TA F_{max}	-50% GAS l_0	-20% SOL l_0		
-60% TA F_{max}			GAS $a_{min} = 0.2$	SOL $a_{min} = 0.1$
	-50% GAS l_0	-10% SOL l_0	GAS $a_{min} = 0.2$	SOL $a_{min} = 0.1$

2.3.3. Validation

The equinus gait simulations selected in the sensitivity analysis were validated with a clustered data set of 56 CP patients with a wide variety of gait patterns, walking overground at self-selected speed, from Toro et al., 2007 [3]. Only the clusters from equinus gait types were selected for the validation. Simulated and experimental hip, knee and ankle angles were compared over the gait cycle using the same similarity metrics from the validation of unimpaired gait in Section 2.2: RMSE and NCC. If the RMSE was lower than 2 SD and the NCC was higher than 0.5, it meant the model could capture experimental trends and therefore used in the following steps with the AFO-assisted gait simulations.

2.4. AFO model

To compensate for increased passive stiffness, the actual AFO applies an exponential torque as a function of the ankle angle (Eq. 2.2, from Rodriguez et al., 2018 [11]), with c_1, c_2, c_3 constant parameters to compensate for stiffness of several patients with equinus (Fig. 2.5, left panel).

$$T_{AFO}(\theta) = c_1 e^{c_2(\theta - c_3)} \tag{2.2}$$

To simulate the effect of the negative stiffness in the model, the AFO was modelled with the OpenSim Expression Based Point To Point Force Tool, that applies a force (F) between two points on the skeletal segments, with a magnitude depending on the distance (d) between these two points: $F = F(d)$. The application points of the AFO force were the attachment points of the right SOL, on the shank and the foot, so that a torque was generated around the right ankle joint (Fig. 2.5, right panel). The force increased exponentially in dorsiflexion, as the distance between the two attachment points of the SOL increased (Eq. 2.3), with a and b constant parameters to compensate for the increased stiffness in the model, resulting from structural and/or neural alterations.

$$F(d) = ae^{bd} \tag{2.3}$$

To simulate the weight of the AFO, an extra weight of 700 g was added, distributed on the right shank and the foot (500 g on the tibia, 100 g on the talus, 100 g on the calcaneus), and the center of mass of the right tibia was moved distally, because the

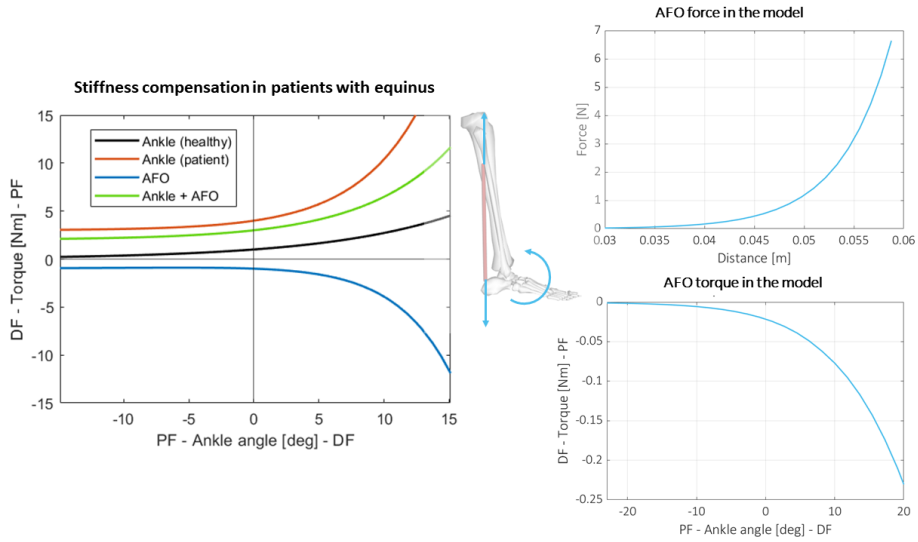

Figure 2.5: Left: Passive ankle joint stiffness is not constant but increases with the angle of rotation in the sagittal plane: from plantarflexion (PF) to dorsiflexion (DF). To compensate for the increased passive ankle joint stiffness of the patient with equinus (red) towards healthy values (black), the ankle-foot orthosis (AFO) applies an external torque (blue) with an exponential function that approximates patient ankle stiffness. The combined stiffness (patient + AFO, green) is reduced towards healthy values. Adapted from Rodriguez et al. 2018 [11]. Right: in the model, stiffness compensation is introduced with a force acting between two points on the shank (top), resulting in a torque around the ankle joint (bottom).

mechanism, heaviest part of the AFO, was placed near the ankle. To simulate the ROM of the AFO, ankle angle limits were set to 60 degrees in plantarflexion and 20 degrees in dorsiflexion.

2.4.1. AFO-assisted gait simulations

The AFO model was tested on two gait simulations that resulted in joint kinematics similar to CP patients with equinus (validation 2.3.3). Resulting ankle angles were compared over time between the equinus gait simulations (without AFO) and equinus gait simulations with AFO (AFO-assisted gait simulations). AFO-assisted gait simulation were expected to result in lower maximum plantarflexion angle and increased ankle ROM.

3

Results

3.1. Unimpaired gait simulation

Results of the validation of kinematic and kinetic trajectories (joint angles, joint moments and GRFs) and muscle activations (GAS, TA, SOL) with experimental data of healthy gait reported by Bovi et al. 2011 [28] and Perry et al., 1992 [30] are shown in Fig. 3.1 and Table 3.1.

For the majority of the gait cycle, all simulated kinematic and kinetic trajectories were within 2 SDs of experimental data [28], except for the knee extension moment. For every trajectory except the knee moment, RMSE between the simulated and experimental data was no more than 1.23 SD, and NCC was at least 0.96 for each trajectory except the ankle dorsiflexion angle and the knee extension moment, (Table 3.1). The low NCC for the ankle joint angle was due to insufficient plantarflexion at toe off, resulting from the restriction of angular velocity. The high RMSE and low NCC for the knee joint moment were due to a high knee flexion moment during the second half of stance, resulting from the force applied to keep the knee DOF from getting out of range, i.e. prevent knee hyperextension.

Similarly to experimental EMG [30], TA activity was higher at loading response (to control foot landing) and in swing (to control foot clearance), while GAS and SOL were most active during the second half of the stance phase (to propel the body forward towards toe-off), but later in the simulation than observed in experiments.

3.2. Equinus gait simulations

3.2.1. Sensitivity analysis

The results on the ankle kinematics due to the alterations (Tables 2.2 and 2.3) on the NMS model are shown in Fig. 3.2. Equinus gait, with toe-strike and abnormal ankle plantarflexion during swing, was obtained in eight simulations (5 with isolated alterations, and the 3 combinations). The 5 isolated alterations were: decreased GAS optimal fiber length, increased GAS minimum activation (Fig. 3.3), GAS

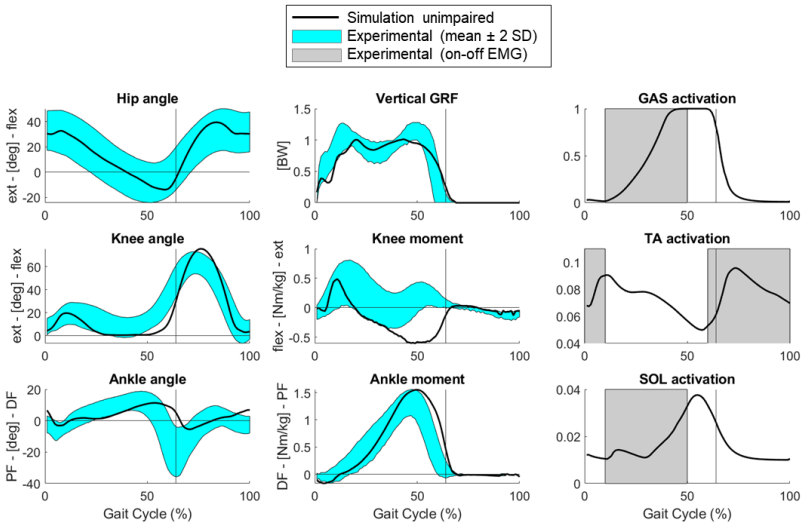

Figure 3.1: Simulated kinematics (hip, knee, ankle angles) and kinetics (knee, ankle moments and vertical ground reaction forces) compared to experimental data of healthy subjects walking at self selected speed, collected by Bovi et al. 2011 [28]. Gastrocnemius (GAS), Tibialis Anterior (TA), Soleus (SOL) muscle activations compared to on-off timings estimated from experimental electromyograms (EMG) reported by Perry et al., 1992 [30]. Toe-off on the vertical line. All simulated kinematics and kinetics were with 2SDs of experimental data for the majority of the gait cycle, except the knee moments. Simulated and experimental TA was active at loading response to control foot landing, and in swing, to control foot clearance. Simulated GAS and SOL were most active during the second half of stance, to propel the body forward towards toe-off, but later than observed in experiments.

Table 3.1: Similarity metrics between simulated and experimental kinematics and kinetics [28] for unimpaired gait: root-mean-squared errors (RMSE), reported in units of standard deviation (SD), and normalized cross correlations (NCC). Low NCC for the ankle angles was due to insufficient plantarflexion at push off. Knee moments deviate the most from experimental data, with the highest RMSE and lowest NCC, due to excessive flexion moment in stance.

	Angles			Moments		Vertical
	Hip	Knee	Ankle	Knee	Ankle	GRF
RMSE [SD]	0.02	0.72	1.23	2.17	1.15	0.19
NCC	0.99	0.95	0.33	-0.07	0.96	0.98

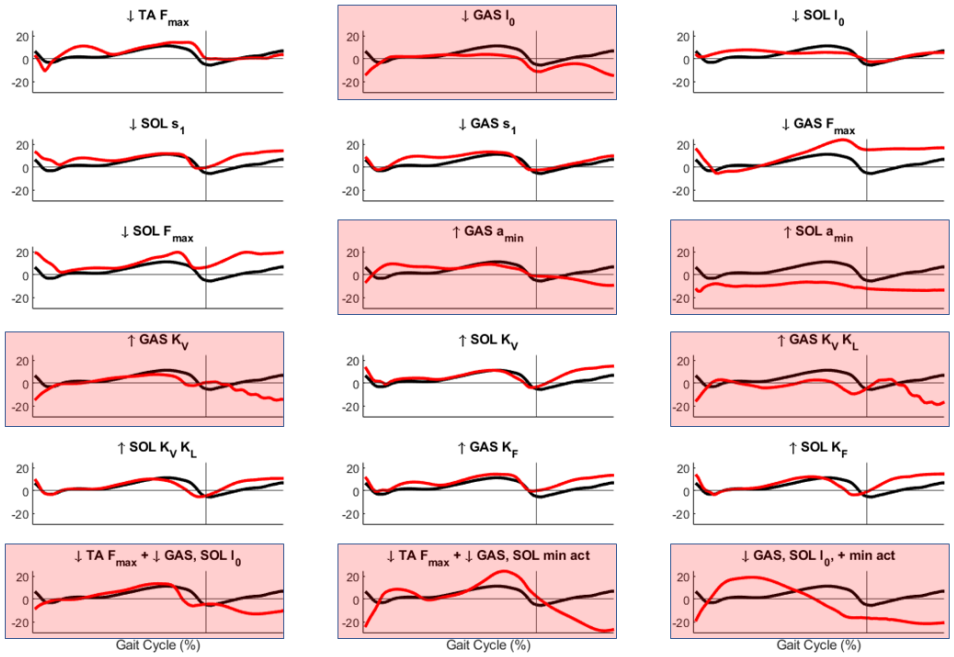

Figure 3.2: Effect of isolated (first 5 rows) and combined (last row) structural and neural alterations of Tibialis Anterior (TA), Gastrocnemius (GAS) and Soleus (SOL), on the ankle angles (black line: unimpaired simulation, red line: altered simulation at highest level) during the gait cycle (toe-off on the vertical line), positive angles, in degrees, are defined in dorsiflexion direction. The eight simulations that resulted in abnormal plantarflexion in swing and toe-strike (equinus gait) are highlighted with red. Abbreviations in the titles: $\downarrow F_{max}$ = decreased maximum isometric force; $\downarrow l_0$ = decreased optimal fiber length; $\downarrow s_1$ = decreased passive strain; $\uparrow a_{min}$ = increased minimum activation; $\uparrow K_V, K_L, K_V$ = increased velocity, length, force feedback.

velocity feedback, velocity and length feedback (Fig. 3.4), increased SOL minimum activation (Fig. 3.5). The 3 combinations were decreased TA maximum isometric force, and/or decreased GAS and SOL optimal fiber lengths and/or increased GAS and SOL minimum activations (Fig. 3.6). In general, the equinus was usually shown together with an increase of hip and knee flexion, or knee hyperextension, and increased ankle plantarflexion moments in stance. The simulations with the addition of GAS velocity feedback also resulted in rapid oscillations of the ankle (clonus) during swing (Fig. 3.4).

The other 10 alterations did not result in equinus gait, with similar or increased dorsiflexion during swing: decreased TA maximum isometric force, decreased SOL optimal fiber length, SOL increased passive stiffness, GAS increased passive stiffness, decreased GAS maximum isometric force, decreased SOL maximum isometric force, SOL velocity feedback, SOL velocity and length feedback, GAS force feedback, SOL force feedback.

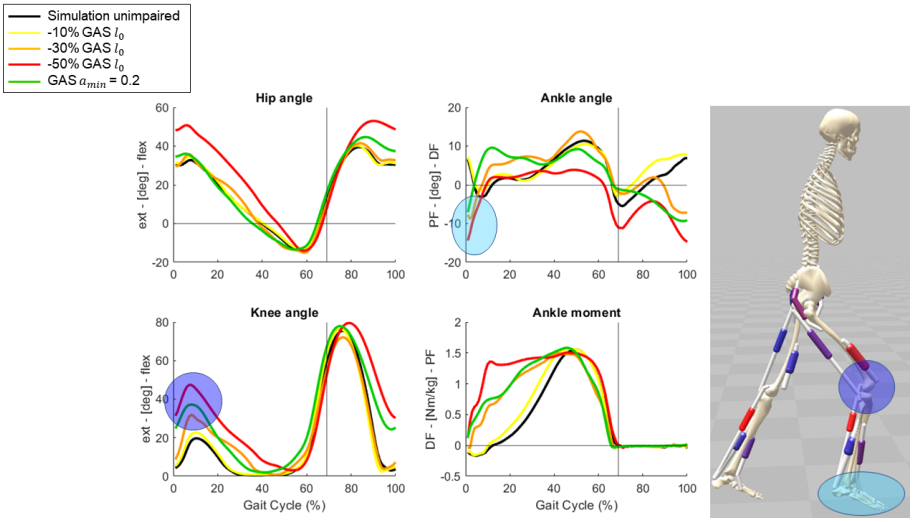

Figure 3.3: Joint kinematics of the right leg and right ankle moments of the simulations that resulted in equinus gait with decreased Gastrocnemius (GAS) optimal fiber length (l_0) or increased GAS minimum activation (a_{min}). With the maximum decrease of GAS optimal fiber length (red line) and minimum activation of 0.2 (green line), the model landed on the forefoot, and showed increased plantarflexion during swing (top right graph). Ankle moments increased at early stance (bottom right graph), and with a "double-bump" pattern in the simulation with the shortest GAS. The knee was flexed during stance (bottom left graph). Hip kinematics (top left graph) remained close to normal, except with the maximum decrease of GAS optimal fiber length.

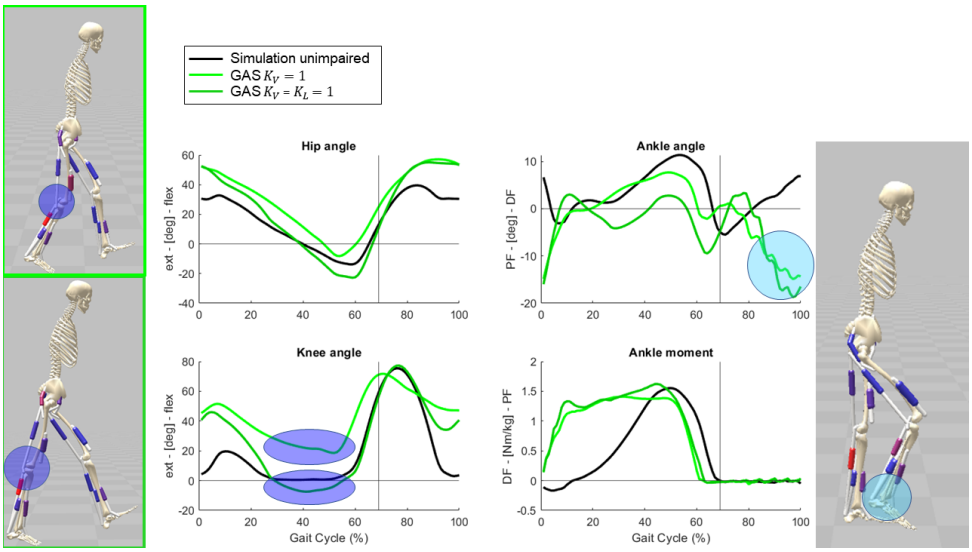

Figure 3.4: Joint kinematics of the right leg and right ankle moments of the simulations that resulted in equinus gait with the addition of only velocity (K_V) and both velocity and length (K_V, K_L) feedback (spastic) reflexes on the right Gastrocnemius. The model showed increased plantarflexion of the ankle joint during the whole gait cycle (top right graph), with the forefoot making contact with the ground at initial contact and rapid oscillations during swing (light blue circle). Ankle moment increased during the first half of stance, with a "double-bump" pattern for the simulation with both velocity and length feedback (bottom right graph). At the knee joint (bottom left graph), the model showed increased flexion in early stance and in late swing, increased flexion or knee hyperextension in the second half of stance (blue circles). At the hip joint (top left graph), the model showed increased flexion in early stance and late swing.

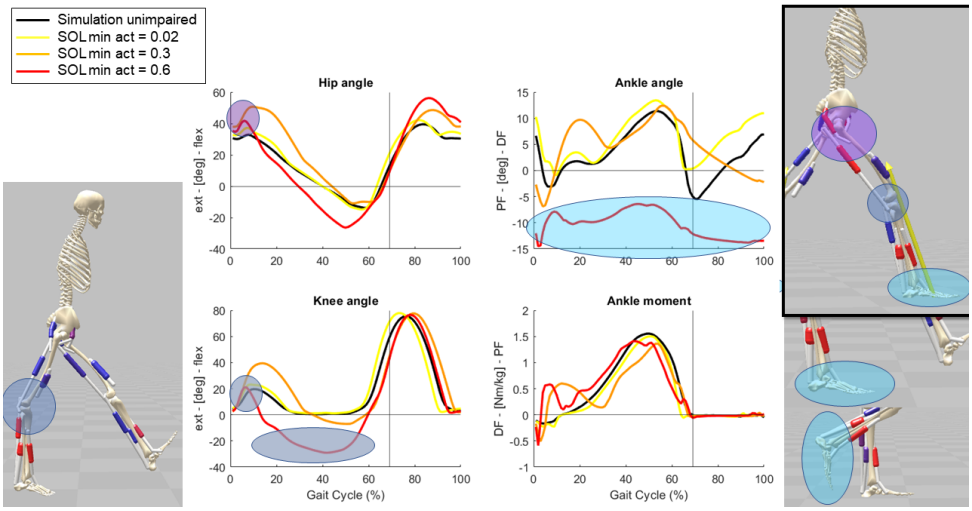

Figure 3.5: Joint kinematics of the right leg and right ankle moments of the simulations that resulted in abnormal plantarflexion with increased minimum activation of the right Soleus. With the maximum increase (red line), the model showed a consistent plantarflexion of the ankle joint during the whole gait cycle (top right graph, light blue circles). The model took long steps, landing with the foot flat, and just after initial contact the hip and knee flexed (blue and lilac circles). Peak ankle moments (bottom right graph) remained similar to normal values. At the knee joint, the model showed high hyperextension throughout stance (bottom left graph, blue circles).

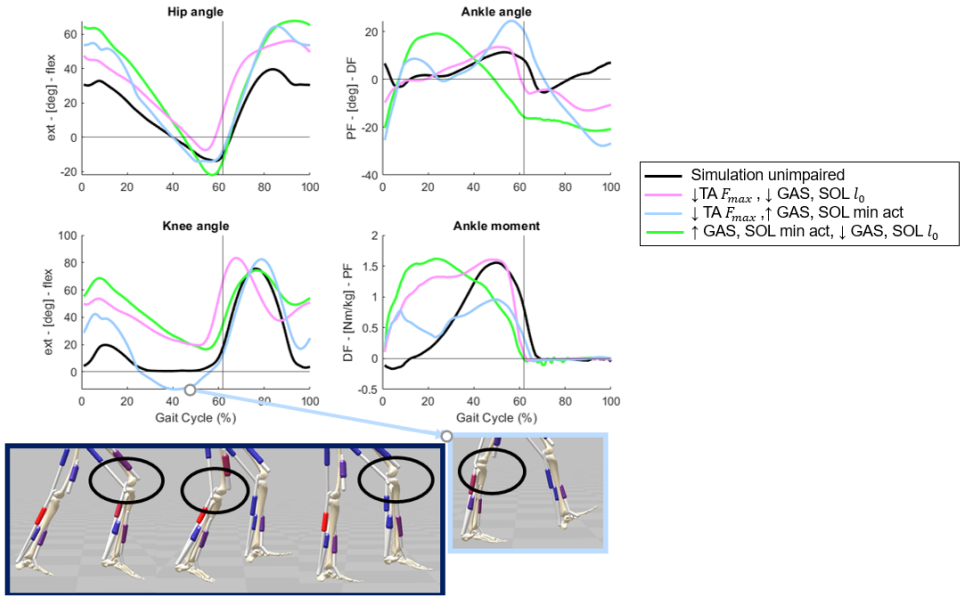

Figure 3.6: Joint kinematics of the right leg and right ankle moments of the simulations that resulted in equinus gait with combinations of decreased maximum isometric force (F_{max}) of Tibialis Anterior (TA) and/or decreased optimal fiber length (l_0) of Gastrocnemius (GAS) and Soleus (SOL), and/or increased minimum activation of GAS and SOL. Hip flexion (top left graph) increased in swing and early stance in all combinations. The knee (bottom left graph) remained flexed during the whole gait cycle (screenshot black panel), except for hyperextension in the simulation with decreased maximum isometric force of TA and increased minimum activation of GAS and SOL (screenshot blue panel). Ankle plantarflexion (top right graph) increased in all combinations, with the forefoot making initial contact with the ground. The ankle moment (bottom right graph) increased in stance in all the combinations, but the peak at push off decreased in the simulation with decreased maximum isometric force of TA and increased minimum activation of GAS and SOL.

3.2.2. Validation

The results of the validation of hip, knee and ankle kinematics of the equinus gait simulations with experimental data from CP patients with equinus reported by Toro et al., 2007 [3] are presented in Figures 3.7 and 3.8. Within the 15 altered simulations, only the 8 simulations that actually resulted in equinus gait features (increased plantarflexion and toe-strike) were validated. Ankle kinematics of all the simulations fell within the experimental range for the majority of the gait cycle (RMSE lower than 2 SD, except for the simulation with increased GAS minimum activation, that resulted in higher dorsiflexion). Ankle kinematics of 4 simulations were not similar in shape to experimental trajectories (NCC lower than 0.5), lacking plantarflexion at push off: increased GAS minimum activation, increased GAS velocity feedback, combinations of decreased TA maximum isometric force and decreased GAS and SOL optimal fiber length; decreased TA maximum isometric force and increased minimum activation of GAS and SOL. Experimental and simulated knee angles were the most similar, with RMSE lower than 2 SD and NCC higher than 0.5 for all trajectories, except for the excessive knee hyper-extension resulted from the increase of the SOL minimum activation. Two simulations showed higher knee flexion than experimental at initial contact: the one with decreased TA maximum isometric force and decreased GAS and SOL optimal fiber length, and the one with decreased optimal fiber length and increased minimum activation of GAS and SOL. Experimental and simulated hip kinematics were similar in shape (NCC higher than 0.5 for all trajectories), however 6 simulations showed higher hip flexion than experimental (with RMSE higher than 2 SDs): decreased GAS optimal fiber length, GAS velocity, velocity and length feedback, and the three combinations.

			Hip angle	Knee angle	Ankle angle
	-50% GAS l_0	RMSE [SD]	2.83	0.19	1.51
		NCC	0.86	0.93	0.56
	GAS a_{min}=0.2	RMSE [SD]	1.40	0.33	2.13
		NCC	0.95	0.97	-0.11
	SOL a_{min}=0.6	RMSE [SD]	0.79	3.20	0.42
		NCC	0.98	0.64	0.90
	GAS K_V=1	RMSE [SD]	3.47	1.35	1.73
		NCC	0.85	0.97	0.26
	GAS K_V =K_L=1	RMSE [SD]	2.00	0.74	1.33
		NCC	0.94	0.91	0.60

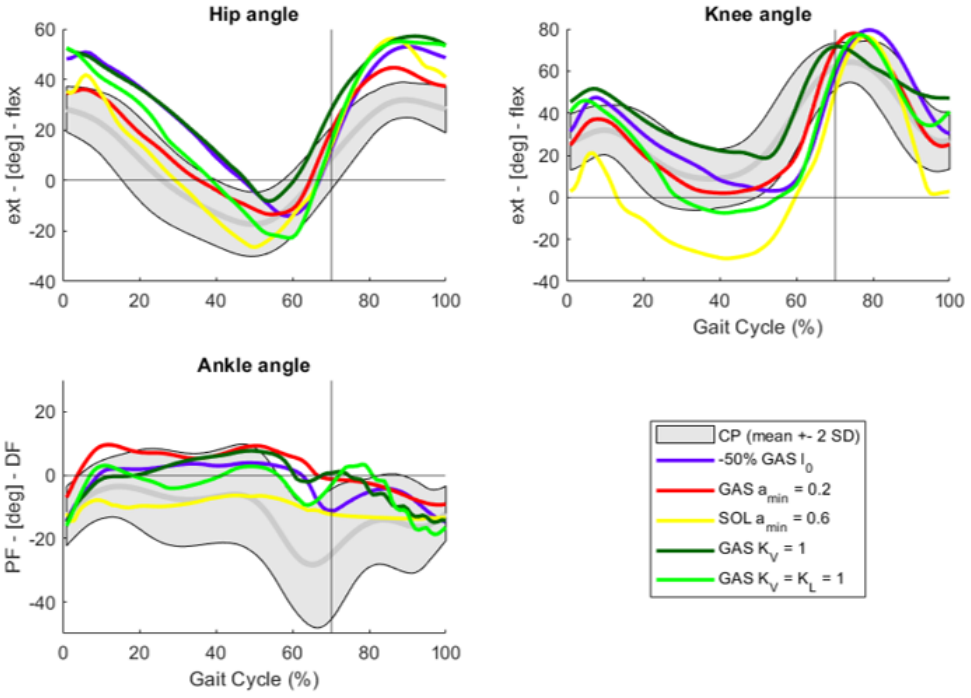

Figure 3.7: Validation of the simulated joint kinematics with isolated alterations of Gastrocnemius (GAS) optimal fiber length (l_0), GAS minimum activation (a_{min}), Soleus (SOL) minimum activation, GAS velocity feedback (K_V) or velocity and length feedback (K_V, K_L), with joint kinematics of Cerebral Palsy (CP) patients with equinus reported by Toro et al. 2007 [3]. Root-mean-squared errors (RMSE) in units of standard deviation (SD) and normalized cross correlations (NCC) are reported in the table. RMSE higher than 2 SD and NCC lower than 0.5 are highlighted with red. Similar to CP patients, ankle angles in the simulations showed high plantarflexion, falling within the experimental range for the majority of the gait cycle, except from the simulations with increased GAS activation or velocity feedback. Both experimental and simulated knee angles showed high flexion, except for the simulation with increased SOL activation, with excessive knee hyper-extension. Simulated hip kinematics reproduced experimental trends (NCC higher than 0.5), but the simulations with altered GAS length or feedbacks showed higher hip flexion (RMSE higher than or equal to 2).

			Hip angle	Knee angle	Ankle angle
	↓TA F_{max}, ↓GAS, SOL l_0	RMSE [SD]	3.58	1.46	1.76
		NCC	0.83	0.95	0.28
	↓TA F_{max}, ↑GAS, SOL a_{min}	RMSE [SD]	2.94	1.16	1.93
		NCC	0.92	0.88	0.04
	↑GAS, SOL a_{min}, ↓GAS, SOL l_0	RMSE [SD]	3.72	1.88	1.16
		NCC	0.88	0.93	0.59

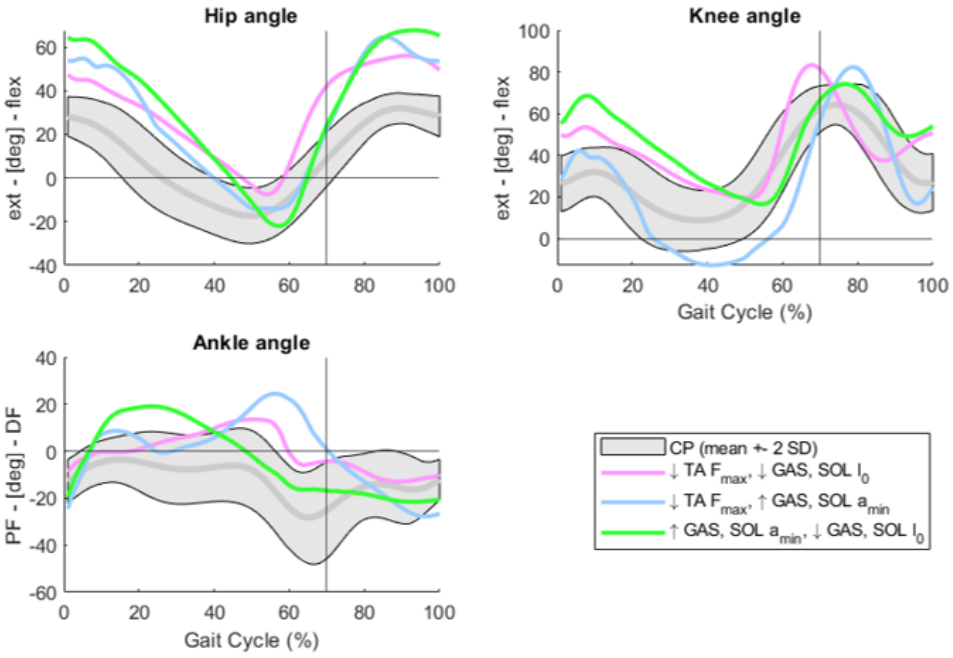

Figure 3.8: Validation of the simulated joint kinematics with combined alterations - decreased Tibialis Anterior (TA) maximum isometric force (F_{max}), and/or shorter Gastrocnemius (GAS) and Soleus (SOL) optimal fiber length (l_0), and/or increased minimum activation (a_{min}) of GAS and SOL- with joint kinematics of Cerebral Palsy (CP) patients with equinus reported by Toro et al. 2007 [3]. Root-mean-squared errors (RMSE) in units of standard deviation (SD) and normalized cross correlations (NCC) are reported in the table. RMSE higher than 2 SD and NCC lower than 0.5 are highlighted with red. Similar to CP patients, simulated knee and ankle angles showed high flexion and plantarflexion, respectively. Ankle NCC was lower than 0.5 for the simulations with decreased TA force, due to lack of plantarflexion at push off. Simulated hip angles followed experimental trends (NCC higher than 0.83), but with higher hip flexion values (RMSE higher than 2 SD).

3.3. AFO-assisted gait simulations

The AFO model was applied on two simulations, one from the isolated structural alterations and one from the combinations of structural and neural alterations, that resulted in joint kinematics similar to CP patients with equinus (validation 3.2.2):

- Case 1: 50% decrease of right GAS optimal fiber length.
- Case 2: 60% decrease of maximum isometric force of right TA and increased minimum activation of right GAS and SOL (0.2 and 0.1 respectively).

The following AFO parameters were used to decrease ankle stiffness: $a = 6.131 * 10^{-5}$, $b = 197.3$ (Eq. 2.3, Fig. 2.5). To determine the parameters repeated varied attempts were performed (Appendix 5).
Both AFO-assisted gait simulations ran for less than 5 seconds, meaning that more iterations in the optimization, and/or adjustments of the AFO model, are needed. Both AFO-assisted gait simulations resulted in reduced equinus, decreasing the maximum ankle plantarflexion angle by 3.2 degrees in Case 1 and 19.2 degrees in Case 2. In Case 1, the maximum dorsiflexion angle also increased by 5.4 degrees, thus the total ankle ROM increased slightly, by 2.2 degrees. In Case 2, on the contrary, the maximum dorsiflexion angle decreased by 15.6 degrees, reducing total ankle ROM by 34.8 degrees.

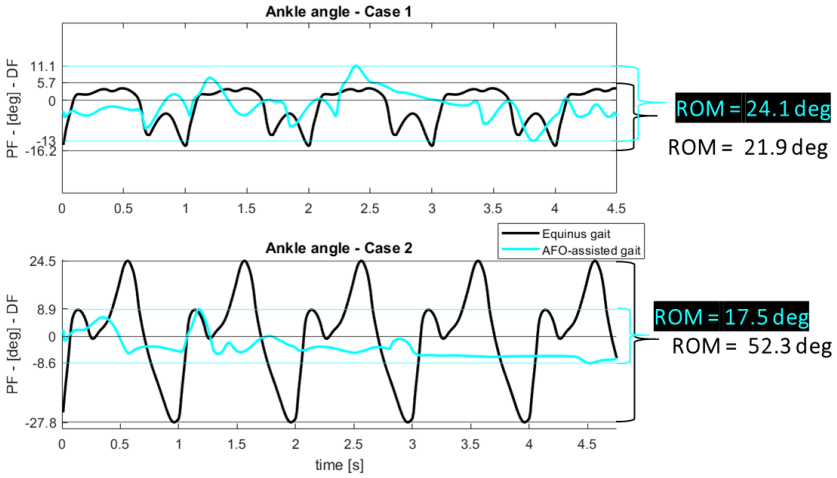

Figure 3.9: Simulated effect of the AFO (red line) on ankle range of motion (ROM) during two gait simulations that resulted in equinus gait (blue line): Case 1 gait simulation with shorter Gastrocnemius, Case 2 gait simulation with weaker Tibialis Anterior and hyperactive plantarflexors. The AFO decreased the maximum plantarflexion angle in both cases, reducing equinus. In Case 1, the AFO increased ankle ROM by 2.2 degrees, while in Case 2 ankle ROM decreased by 34.8 degrees.

4

Discussion

The goal of this study was to generate forward simulations of equinus gait with a NMS model, that included both muscular and neural alterations that contribute to increased ankle joint stiffness, and predict the effects of ankle stiffness compensation with an AFO model. Firstly, a simulation of unimpaired gait was generated and validated, in order to start with a reliable model. Secondly, it was found that several isolated and combined structural and neural alterations of the muscles around the ankle joint caused the model to adopt an equinus gait, similar to that of CP patients with equinus, e.g., toe-strike, abnormal plantarflexion during swing, increased knee and hip flexion or knee hyperextension on the affected side. Finally, the AFO, modelled as an external torque around the ankle, compensated the ankle joint stiffness, caused by the neural and structural alterations introduced in the NMS model, by decreasing ankle plantarflexion, and increasing ankle ROM in the condition with shorter GAS.

4.1. Unimpaired gait simulation

The unimpaired gait simulation built upon previous simulations of gait with additional measures generated realistic results that could be validated. Quantitative validation of hip, knee, ankle angles, knee and ankle moments, and vertical GRFs with data from literature showed that the simulation was able to capture the experimental trends. Only the knee joint moments did not follow experimental trends, with excessive flexion moments in stance, when the GRF passed in front of the knee, generating an external extension moment, and requiring the generation of an opposing internal muscle moment to control knee motion and prevent knee hyperextension. The simulated ankle angles did not reach the same plantarflexion peak at toe-off as the experimental values, most likely because the measures that restricted ankle velocity, to prevent abnormal rapid plantarflexion at initial contact, also prevented normal plantarflexion at push off. Qualitative validation of TA, GAS and SOL muscle activations with experimental EMG on-off timings showed that the

simulated muscle activities captured many salient features observed in experiments, such as TA activation throughout swing, to control foot clearance, and at loading response, to control foot landing, and plantarflexors activation in stance, to propel the body forward towards toe-off. However, there were some differences between simulations and experimental EMG, such as later onset times for the plantarflexors, activation of the TA during the whole gait phase and only GAS activation reaching 100% activation, likely due to the choice of the energy model to compute effort.

The objective function contained terms that are thought to capture the general goals of human walking, such as maximize walking speed, minimize energy consumption, and avoid injury, however a trade-off between the competing objectives likely varies between individuals. The objective function may not totally represent the goals of individuals with gait pathologies and/or walking with the AFO. It is unclear what is optimized in pathological walking [49], for example, impaired individuals may choose a trade-off between metabolic efficiency, stability and pain avoidance. Additional measures (limiting vertical GRF, ankle velocity, hip displacement, stride duration and length) did not capture goals of walking, and were rather included to remove abnormal dynamics likely caused by the contact model and generate more realistic results. The contact model applied contact forces between two elements, the feet and the ground, taking deformations of both elements into account, based on linear elasticity theory [50] and probably generated too stiff contacts, resulting in abnormal peaks of vertical GRF and rapid abnormal plantarflexion at initial contact. GRF and plantarflexion angles improved with the introduction of the additional measures.

The model used in the simulations included a limited number of muscles. Although inclusion of many muscles is more realistic from a physiological perspective, it is not necessary in order to simulate gait in the sagittal plane. Moreover, a higher number of muscles requires a higher number of model parameters to be optimized, therefore longer computational time to find the optimal solution.

4.2. Equinus gait simulations

The simulations of equinus gait of the present study was unprecedented for two reasons. First, because the simulations included both altered muscular structural properties and neural alterations that contribute to increased ankle joint stiffness of patients with equinus, overcoming the limitations of previous forward simulations [15–17, 20]. Second, because both alterations were applied during gait, instead of passive muscle stretches like in previous studies [18, 19, 21]. These advantages derive from the use of a NMS model that includes both a neural model (gait controller) and musculoskeletal model.

Sensitivity analysis

The model was robust to all alterations, finding a stable gait in all cases. Sensitivity analysis showed that shortening or spasticity of the GAS, or SOL hyperactivity, or combinations of plantarflexor muscles shortening and/or hyperactivity with TA weakness influenced the most ankle kinematics, and caused equinus gait, with excessive ankle plantarflexion, toe-strike at first contact, and abnormal ankle moments.

Alterations of the muscles around the ankle joint did not only have a local effect on the ankle kinematics, but also resulted in altered hip and knee kinematics, with increased hip and knee flexion in late swing and early stance, or knee hyperextension in mid stance. The simulation with GAS velocity feedback also resulted in unexpected ankle clonus, with rhytmic muscle contractions of the GAS and oscillatory movements of the ankle during swing. Ten alterations (of TA, GAS or SOL force, SOL length, SOL or GAS passive stiffness, 3 SOL feedback gains, GAS force feedback gain) did not result in equinus gait, with same or higher dorsiflexion angles and heel strike at initial contact, and therefore were not validated.

Validation

Quantitative validation of the equinus gait simulations was a crucial step to prove that the present model was a starting point for the AFO-assisted gait simulations. However, it was impractical to validate each simulation with isolated neuromuscular alterations with experimental data of patients with the same deficits (e.g. simulation with decreased GAS optimal fiber length with patients with shorter GAS muscles) because patients usually show a combination of neuromuscular deficits, and also because many the studies did not provide their collected data sets. Therefore, all the simulations that resulted in abnormal plantarflexion were validated with kinematic data from patients with equinus, target population of the new AFO. A previously collected data set of CP patients with a wide range of gait patterns was selected for validation. The data set was divided into clusters, and only the clusters with equinus were selected.

Overall, the simulations well captured the pathological toe-walking pattern, commonly seen in CP patients, characterized by abnormal plantarflexion and increased knee flexion throughout stance. Experimental and simulated knee angles were the most similar in shapes and values, with low RMSE and high NCC, with the only exception of the simulation with increased SOL activation, that showed excessive knee hyperextension. Experimental and simulated ankle angles were similar in values, with low RMSE (except for the simulation with increased GAS activation), but not always in shape, with low NCC for simulations with increased GAS activation or velocity feedback, or combinations with decreased TA force. Hip angles trajectories had low NCC, but high RMSE, meaning they reproduced well experimental trends, but with values deviating from the experimental mean. In fact, the model took long steps, with high hip flexion at terminal stance and initial contact. The model taking longer steps could be a secondary effect of trying to clear the foot off the ground, being the movement restricted to the sagittal plane.

Unfortunately, quantitative validation with CP showed that none of the simulations totally fit with experimental data with respect to all joints, with RMSE higher than 2 SD and/or NCC lower than 0.5 for at least one joint (hip, knee, ankle). However, similarities with gait patterns commonly seen in other patient populations suffering from neuromuscular disorders were recognized, even though they were not used for quantitative validation, due to lack of data. For example, although the model showed higher hip flexion angles than CP children, angles were in the range of healthy adults walking with equinus constraint [4]. Loss of heel strike at initial contact, and re-

duced dorsiflexion was also reported in patients with plantarflexor contractures [51] and hemiparetic stroke patients [52]. Increased knee flexion at initial contact and throughout stance was observed in people with plantarflexor contractures [51, 53], after stroke [1, 52], and CP patients with crouch gait [54]. Knee hyperextension during stance, or knee recurvatum, was often reported in stroke, traumatic brain injury, CP, poliomelitis and multiple sclerosis patients [55]. Decreased ankle moments, resulting from the simulation with TA weakness and plantarflexor hyperactivity, were also reported after stroke [40, 52, 56] and in Charcot-Marie-Tooth-Disease patients with muscle weakness [57]. Increased ankle moment during the first part of stance phase and the "double-bump" ankle moment pattern, with a plantar flexion moment peak during the loading response (resulting from the simulations with GAS shortening or spasticity) was measured in patients with plantarflexor contractures [51, 53], spasticity in the calf muscles [56] and healthy subjects walking on their toes [4, 58]. Clonus at the ankle is closely linked to spasticity and the results of this study support the hypothesis that it is caused by self-excitation mechanisms [59]: in the spasticity model, in fact, GAS excitation is computed using a feedback term based on GAS velocity.

The ten alterations introduced that did not result in increased ankle plantarflexion, i.e., equinus gait, were excluded from the validation. When TA, GAS or SOL muscle weakness was introduced, the model achieved similar ankle kinematics due to compensation with increased activations of the weakened muscles, in line with previous studies of NMS modelling of muscle weakness [60, 61]. This compensation allowed for a decrease of GAS maximum isometric force until zero, with increased SOL activation, and viceversa. Similar compensations happened with the increase of SOL or GAS passive stiffness, consistently with experimental observations of stroke patients with high plantarflexion stiffness, who achieved normal dorsiflexion angles during swing due to increased TA activation [62]. Simulated spasticity of the SOL muscle, with additional reflexes based on muscle length, velocity, or force, did not result in equinus gait, supporting previous hypotheses that SOL muscle spasticity is unlikely to contribute to equinus gait in CP children [63].

Limitations

Lack of DOF and muscles did not allow for all commonly observed compensations in patients that are out of the sagittal plane, such as hip abduction and/or circumduction and pelvic tilt. Stiff knee gait, usually observed in patients after stroke or CP, with insufficient or delayed knee flexion during swing [52, 64], did not result from any of the simulations, but it could result from other NMS alterations, such as spasticity of the knee extensors or decreased plantarflexors and hip flexors strength.

Outputs of the gait simulations with neural and structural alterations were joint angles and ankle moments, because in clinical practice the observation of impaired gait most commonly focuses on kinematics, and kinetic measures are also evaluated to connect abnormal movement to underlying muscle malfunction [56]. Knee moments were not included in the outcomes of the sensitivity analysis and validation because the results of the unimpaired gait simulation were not validated with experimental data (Tab. 3.1). Muscle activations were affected by the alterations, because the

approach to evaluate sensitivity involved re-optimization of the neural controller, in which muscle activations were re-calculated after each muscle parameter was perturbed. However, muscle activations were not included in the outputs of the equinus gait simulations because of lack of available data for validation.

4.3. AFO-assisted gait simulations

The AFO model applied an external torque on the ankle joint that increased exponentially with the dorsiflexion angle, resembling the action of the real AFO. Despite the short simulation time, resulting ankle angles during the first 4 or 5 steps could be analyzed. Stiffness compensation by an external dorsiflexion torque provided a beneficial effect by reducing the maximum plantarflexion angle of the two selected simulations of equinus gait. The simulation with shorter GAS length resulted in a beneficial increase of total ankle ROM, while the simulation with weaker TA and hyperactivity of GAS and SOL resulted in a detrimental restricted ankle ROM, with the ankle maintaining a position close to neutral throughout the whole gait cycle, similar to the effect of a passive rigid AFO. The results of the AFO-assisted gait simulations did not totally support the hypothesis of increased active ankle ROM, benefit that the negative stiffness AFO theoretically provides [11]. The reason could be that the AFO does not provide enough stiffness compensation, due to the low torque, and/or the optimization did not find the optimal solution. From clinical experience, however, the effects of the AFOs vary from patient to patient, and some patients will not walk with an increased ankle ROM even if the AFO allows it, because they adopt different gait compensations at the knee and hip.

Limitations and future recommendations

The AFO model applied a force between the two attachment points of the SOL, however, due small moment arms, between 4 and 5 cm, the resulting torques were lower than the torques applied by the actual AFO, resulting in under compensation of the ankle stiffness. The present AFO model should be improved, by directly applying a torque as a function of the ankle angle, and achieve higher compensation. The AFO-assisted gait simulations run for less than 10 seconds, meaning that the solutions provided here are unlikely to be the global minima. Using different CMA-ES parameters, such as larger population size, higher number of iterations and smaller minimum progress, may result in stable gait simulations and different ankle angles than those found in this study. Selecting simulations of equinus resulting from other neural and/or structural alterations may lead to different gait compensations, and future work to test them would be valuable. Suggestions for a more realistic AFO model can be made: the present AFO model added weight on the shank and the foot body segments, but it would be more realistic to model an external body that replicates the shape and material properties of the AFO, and also add a model of the shoe. Despite these limitations, two-dimensional modelling represents a useful initial approach to isolate AFO effects during gait and investigate the effects of ankle stiffness compensation.

The new AFO has not yet been tested on a clinical population of patients with equinus, therefore predicting its effect on equinus gait simulations is important at this stage of the device development. However, future research should focus on the validation of the AFO-assisted gait simulations with gait data from patients with equinus walking with the AFO. Moreover, collected data will be used to define a patient specific NMS model, with specific alterations in muscle and neural properties. Results can ultimately assist in the prescription of the AFO with the optimal settings for the specific patient. All the gait simulations with neuromuscular alterations can also be collected in a database to help clinicians recognize impaired gait patterns of new patients, trace the underlying neuromuscular deficits and prescribe the AFO with the optimal settings for each new patient.

5

Conclusion

The goal of this study was to generate forward simulations of equinus gait with a NMS model, that included both muscular and neural alterations that contribute to increased ankle joint stiffness, and predict the effects of ankle stiffness compensation with an AFO model.

To begin with, a two-dimensional simulation of unimpaired gait was successfully validated, reproducing well experimental kinematics, kinetics and muscle activations observed in healthy subjects.

Next, simulations with shorter or spastic GAS, spastic SOL or combinations of weak TA, and shorter or hyperactive plantarflexors resulted in equinus gait, with toe-strike, abnormal plantarflexion during swing, increased knee and hip flexion or knee hyperextension on the affected side. The simulations were quantitatively validated with CP equinus gait and also reproduced gait features observed in other patient populations with ankle impairments.

Finally, AFO-assisted gait simulations predicted that compensating ankle joint stiffness decreased abnormal ankle plantarflexion, and increased ankle ROM in case of GAS shortening.

Further work is recommended to achieve higher stiffness compensation, as the torque applied by the AFO model was too small, generate more AFO-assisted gait simulations and collect new data to validate them. This study provides a solid base for further investigation of the effects of ankle stiffness compensation on equinus gait, and the results can ultimately assist in the prescription of the new AFO with adjustable stiffness, specific for each patient with equinus.

Acknowledgements

I would like to thank my supervisors Jurriaan, Marjon and Winfred for all their help and interesting discussions throughout the entire project. Thank you Karen for your support and revising the report. I wish you all the best. Thank you Thomas for answering my questions and providing me useful insights. And finally, I would like to express my gratitude to the people who were always close to me, also virtually, during the hardest times. Without you, I would have never made it.

References

[1] M. Manca, G. Ferraresi, M. Cosma, L. Cavazzuti, M. Morelli, and M. G. Benedetti, "Gait patterns in hemiplegic patients with equinus foot deformity," BioMed Research International, vol. 2014, 2014.

[2] S. Kinsella and K. Moran, "Gait pattern categorization of stroke participants with equinus deformity of the foot," Gait and Posture, vol. 27, no. 1, pp. 144–151, 2008.

[3] B. Toro, C. J. Nester, and P. C. Farren, "Cluster analysis for the extraction of sagittal gait patterns in children with cerebral palsy," Gait & posture, vol. 25, no. 2, pp. 157–165, 2007.

[4] M. J. Goodman, J. L. Menown, J. M. West Jr, K. M. Barr, D. W. Vander Linden, and M. L. McMulkin, "Secondary gait compensations in individuals without neuromuscular involvement following a unilateral imposed equinus constraint," Gait & posture, vol. 20, no. 3, pp. 238–244, 2004.

[5] M. Goldstein and D. C. Harper, "Management of cerebral palsy: equinus gait," Developmental medicine and child neurology, vol. 43, no. 8, pp. 563–569, 2001.

[6] D. A. Hampton, K. W. Hollander, and J. R. Engsberg, "Equinus deformity as a compensatory mechanism for ankle plantarflexor weakness in cerebral palsy," Journal of applied biomechanics, vol. 19, no. 4, pp. 325–339, 2003.

[7] K. L. De Gooijer-Van De Groep, E. De Vlugt, J. H. De Groot, H. C. Van Der Heijden-Maessen, D. H. Wielheesen, R. S. Van Wijlen-Hempel, J. H. Arendzen, and C. G. Meskers, "Differentiation between non-neural and neural contributors to ankle joint stiffness in cerebral palsy," Journal of NeuroEngineering and Rehabilitation, vol. 10, no. 1, p. 1, 2013.

[8] L. Bar-On, G. Molenaers, E. Aertbeliën, A. Van Campenhout, H. Feys, B. Nuttin, and K. Desloovere, "Spasticity and its contribution to hypertonia in cerebral palsy," BioMed Research International, vol. 2015, 2015.

[9] J. Leung and A. M. Moseley, "Impact of ankle-foot orthoses on gait and leg muscle activity in adults with hemiplegia," Physiotherapy, vol. 89, no. 1, pp. 39–55, 2003.

[10] B. Chen, B. Zi, Y. Zeng, L. Qin, and W. H. Liao, "Ankle-foot orthoses for rehabilitation and reducing metabolic cost of walking: Possibilities and challenges," Mechatronics, vol. 53, no. July, pp. 241–250, 2018.

[11] K. Rodriguez, J. De Groot, F. Baas, M. Stijntjes, F. Van Der Helm, H. Van Der Kooijl, and W. Mugge, "Passive Ankle Joint Stiffness Compensation by a Novel Ankle-Foot-Orthosis," Proceedings of the IEEE RAS and EMBS International Conference on Biomedical Robotics and Biomechatronics, vol. 2018-Augus, pp. 517–522, 2018.

[12] C. L. Brockett and G. J. Chapman, "Biomechanics of the ankle," Orthopaedics and Trauma, vol. 30, no. 3, pp. 232–238, 2016.

[13] T. S. Buchanan, D. G. Lloyd, K. Manal, and T. F. Besier, "Neuromusculoskeletal modeling: Estimation of muscle forces and joint moments and movements from measurements of neural command," Journal of Applied Biomechanics, vol. 20, no. 4, pp. 367–395, 2006.

[14] E. S. Arch, S. J. Stanhope, and J. S. Higginson, "Passive-dynamic ankle–foot orthosis replicates soleus but not gastrocnemius muscle function during stance in gait: insights for orthosis prescription," Prosthetics and orthotics international, vol. 40, no. 5, pp. 606–616, 2016.

[15] C. F. Ong, T. Geijtenbeek, J. L. Hicks, and S. L. Delp, "Predicting gait adaptations due to ankle plantarflexor muscle weakness and contracture using physics-based musculoskeletal simulations," PLoS computational biology, vol. 15, no. 10, p. e1006993, 2019.

[16] J. S. Higginson, F. E. Zajac, R. R. Neptune, S. A. Kautz, C. G. Burgar, and S. L. Delp, "Effect of equinus foot placement and intrinsic muscle response on knee extension during stance," Gait and Posture, vol. 23, no. 1, pp. 32–36, 2006.

[17] L. A. Luengas, E. Camargo, and G. Sanchez, "Modeling and simulation of normal and hemiparetic gait," Frontiers of Mechanical Engineering, vol. 10, no. 3, pp. 233–241, 2015.

[18] M. V. D. Krogt and A. Seth, "A model of muscle spasticity in opensim," Gait & Posture, vol. 38, p. S16, 2013.

[19] J. W. Fee and R. A. Foulds, "Neuromuscular Modeling of Spasticity in Cerebral Palsy," IEEE Transactions on Neural Systems and Rehabilitation Engineering, vol. 12, no. 1, pp. 55–64, 2004.

[20] K. Jansen, F. D. Groote, W. Aerts, J. D. Schutter, J. Duysens, and I. Jonkers, "Altering length and velocity feedback during a neuro-musculoskeletal simulation of normal gait contributes to hemiparetic gait characteristics," Journal of NeuroEngineering and Rehabilitation, vol. 11, no. 1, pp. 1–15, 2014.

[21] A. F. Id, L. Bar-on, K. Desloovere, I. Jonkers, and F. D. Groote, "A spasticity model based on feedback from muscle force explains muscle activity during passive stretches and gait in children with cerebral palsy," PLoS ONE, pp. 1–20, 2018.

[22] C. A. Crabtree and J. S. Higginson, "Modeling neuromuscular effects of ankle foot orthoses (AFOs) in computer simulations of gait," Gait and Posture, vol. 29, no. 1, pp. 65–70, 2009.

[23] R. M. and S. K.M., "Simulated impacts of ankle foot orthoses on muscle demand and recruitment in typically developing children and children with cerebral palsy and crouch gait," PLoS ONE, vol. 12, no. 7, pp. 1–19, 2017.

[24] A. Seth, J. L. Hicks, T. K. Uchida, A. Habib, C. L. Dembia, J. J. Dunne, C. F. Ong, M. S. DeMers, A. Rajagopal, M. Millard, S. R. Hamner, E. M. Arnold, J. R. Yong, S. K. Lakshmikanth, M. A. Sherman, J. P. Ku, and S. L. Delp, "OpenSim: Simulating musculoskeletal dynamics and neuromuscular control to study human and animal movement," PLOS Computational Biology, vol. 14, no. 7, pp. 1–20, 2018.

[25] S. L. Delp, F. C. Anderson, A. S. Arnold, P. Loan, A. Habib, C. T. John, E. Guendelman, and D. G. Thelen, "OpenSim: Open-Source Software to Create and Analyze Dynamic Simulations of Movement," IEEE Transactions on Biomedical Engineering, vol. 54, no. 11, pp. 1940–1950, 2007.

[26] T. Geijtenbeek, "SCONE: Open Source Software for Predictive Simulation of Biological Motion," Journal of Open Source Software, vol. 4, no. 38, p. 1421, 2019.

[27] H. Geyer and H. Herr, "A Muscle-reflex model that encodes principles of legged mechanics produces human walking dynamics and muscle activities," IEEE Transactions on Neural Systems and Rehabilitation Engineering, vol. 18, no. 3, pp. 263–273, 2010.

[28] G. Bovi, M. Rabuffetti, P. Mazzoleni, and M. Ferrarin, "A multiple-task gait analysis approach: Kinematic, kinetic and EMG reference data for healthy young and adult subjects," Gait and Posture, vol. 33, no. 1, pp. 6–13, 2011.

[29] T. A. L. Wren, K. P. Do, S. A. Rethlefsen, and B. Healy, "Cross-correlation as a method for comparing dynamic electromyography signals during gait," Journal of Biomechanics, vol. 39, pp. 2714–2718, 2006.

[30] J. Perry, J. R. Davids, et al., Gait analysis: normal and pathological function, vol. 12. LWW, 1992.

[31] S. Dorsch, L. Ada, C. G. Canning, M. Al-Zharani, and C. Dean, "The strength of the ankle dorsiflexors has a significant contribution to walking speed in people who can walk independently after stroke: An observational study," Archives of Physical Medicine and Rehabilitation, vol. 93, no. 6, pp. 1072–1076, 2012.

[32] S. S. Ng and C. W. Hui-Chan, "Contribution of ankle dorsiflexor strength to walking endurance in people with spastic hemiplegia after stroke," Archives of Physical Medicine and Rehabilitation, vol. 93, no. 6, pp. 1046–1051, 2012.

[33] C. S. Klein, G. A. Power, D. Brooks, and C. L. Rice, "Neural and muscular determinants of dorsiflexor weakness in chronic stroke survivors," Motor Control, vol. 17, no. 3, pp. 283–297, 2013.

[34] K. Dragert and E. P. Zehr, "High-intensity unilateral dorsiflexor resistance training results in bilateral neuromuscular plasticity after stroke," Experimental Brain Research, pp. 93–104, 2013.

[35] F. Gao and L.-Q. Zhang, "In vivo biomechanical evaluations of the medial gastrocnemius: changes in muscle properties in stroke survivors," in 2006 International Conference of the IEEE Engineering in Medicine and Biology Society, pp. 2083–2086, IEEE, 2006.

[36] R. F. Frisk, J. Lorentzen, L. Barber, and J. B. Nielsen, "Characterization of torque generating properties of ankle plantar flexor muscles in ambulant adults with cerebral palsy," European Journal of Applied Physiology, vol. 119, no. 5, pp. 1127–1136, 2019.

[37] H. Zhao, Y. Ren, E. J. Roth, R. L. Harvey, and L. Q. Zhang, "Concurrent deficits of soleus and gastrocnemius muscle fascicles and Achilles tendon post stroke," Journal of Applied Physiology, vol. 118, no. 7, pp. 863–871, 2015.

[38] T. A. L. Wren, K. P. Do, and R. M. Kay, "Gastrocnemius and soleus lengths in cerebral palsy equinus gait differences between children with and without static contracture and effects of gastrocnemius recession," Journal of biomechanics, vol. 37, no. 9, pp. 1321–1327, 2004.

[39] V. Dietz, J. Quintern, and W. Berger, "Electrophysiological studies of gait in spasticity and rigidity: Evidence that altered mechanical properties of muscle contribute to hypertonia," Brain, vol. 104, no. 3, pp. 431–449, 1981.

[40] S. Nadeau, D. Gravel, A. B. Arsenault, and D. Bourbonnais, "Plantarflexor weakness as a limiting factor of gait speed in stroke subjects and the compensating role of hip flexors," Clinical biomechanics, vol. 14, no. 2, pp. 125–135, 1999.

[41] P.-y. Lin, "The Relation Between Ankle Impairments and Gait Velocity," Archives of physical medicine and rehabilitation, vol. 87, no. April, pp. 562–568, 2006.

[42] V. Dietz and T. Sinkjaer, "Spastic movement disorder: impaired reflex function and altered muscle mechanics," Lancet Neurology, vol. 6, no. 8, pp. 725–733, 2007.

[43] J. A. Burne and V. L. Carleton, "The spasticity paradox: movement disorder or disorder of resting limbs ?," Journal of Neurology, Neurosurgery and Psychiatry, pp. 47–54, 2005.

[44] J. Perry, M. M. Hoffer, P. Giovan, D. Antonelli, and R. Greenberg, "Gait analysis of the triceps surae in cerebral palsy: a preoperative and postoperative clinical and electromyographic study," JBJS, vol. 56, no. 3, pp. 511–520, 1974.

[45] J. Perry, R. L. Waters, and T. Perrin, "Electromyographic analysis of equinovarus following stroke.," Clinical Orthopaedics and Related Research (1976-2007), vol. 131, pp. 47–53, 1978.

[46] N. J. O'Dwyer, L. Ada, and P. D. Neilson, "Spasticity and muscle contracture following stroke," Brain, vol. 119, no. 5, pp. 1737–1749, 1996.

[47] K. P. Blum, B. Lamotte D'Incamps, D. Zytnicki, and L. H. Ting, "Force encoding in muscle spindles during stretch of passive muscle," PLoS Computational Biology, vol. 13, no. 9, pp. 1–24, 2017.

[48] A. Saltelli, "Sensitivity analysis for importance assessment," Risk analysis, vol. 22, no. 3, pp. 579–590, 2002.

[49] S. J. Piazza, "Muscle-driven forward dynamic simulations for the study of normal and pathological gait," Journal of NeuroEngineering and Rehabilitation, vol. 3, pp. 1–7, 2006.

[50] M. A. Sherman, A. Seth, and S. L. Delp, "Simbody : multibody dynamics for biomedical research," Procedia IUTAM, vol. 2, pp. 241–261, 2011.

[51] S. Armand and M. Attias, Contracture and Gait Deviations, pp. 1–21. Cham: Springer International Publishing, 2018.

[52] S. J. Olney and C. Richards, "Hemiparetic gait following stroke. Part I: Characteristics," Gait and Posture, vol. 4, no. 2, pp. 136–148, 1996.

[53] J. Leung, R. Smith, L. A. Harvey, A. M. Moseley, and J. Chapparo, "The impact of simulated ankle plantarflexion contracture on the knee joint during stance phase of gait: A within-subject study," Clinical Biomechanics, vol. 29, no. 4, pp. 423–428, 2014.

[54] T. A. Wren, S. Rethlefsen, and R. M. Kay, "Prevalence of specific gait abnormalities in children with cerebral palsy: Influence of cerebral palsy subtype, age, and previous surgery," Journal of Pediatric Orthopaedics, vol. 25, no. 1, pp. 79–83, 2005.

[55] D. C. Kerrigan, L. C. Deming, and M. K. Holden, "Knee recurvatum in gait: a study of associated knee biomechanics," Archives of physical medicine and rehabilitation, vol. 77, no. 7, pp. 645–650, 1996.

[56] L. H. Sloot and M. M. van der Krogt, Interpreting Joint Moments and Powers in Gait, pp. 625–643. Cham: Springer International Publishing, 2018.

[57] M. Ferrarin, G. Bovi, M. Rabuffetti, P. Mazzoleni, A. Montesano, E. Pagliano, A. Marchi, A. Magro, C. Marchesi, D. Pareyson, et al., "Gait pattern classification in children with charcot–marie–tooth disease type 1a," Gait & posture, vol. 35, no. 1, pp. 131–137, 2012.

[58] J. Perry, J. M. Burnfield, J. K. Gronley, and S. J. Mulroy, "Toe walking: muscular demands at the ankle and knee," Archives of physical medicine and rehabilitation, vol. 84, no. 1, pp. 7–16, 2003.

[59] I. Boyraz, H. Uysal, B. Koc, and H. Sarman, "Clonus: definition, mechanism, treatment," Med Glas (Zenica), vol. 12, no. 1, pp. 19–26, 2015.

[60] A. S. Fox, C. P. Carty, L. Modenese, L. A. Barber, and G. A. Lichtwark, "Simulating the effect of muscle weakness and contracture on neuromuscular control of normal gait in children," Gait and Posture, vol. 61, no. June 2017, pp. 169–175, 2018.

[61] B. Michalina and A. Wit, "Gait & Posture Compensatory strategy for ankle dorsi fl exion muscle weakness during gait in patients with drop-foot," Gait & posture, vol. 68, pp. 88–94, 2019.

[62] A. Lamontagne, F. Malouin, C. L. Richards, and F. Dumas, "Mechanisms of disturbed motor control in ankle weakness during gait after stroke," Gait and Posture, vol. 15, no. 3, pp. 244–255, 2002.

[63] M. Willerslev-Olsen, J. B. Andersen, T. Sinkjaer, and J. B. Nielsen, "Sensory feedback to ankle plantar flexors is not exaggerated during gait in spastic hemiplegic children with cerebral palsy," Journal of neurophysiology, vol. 111, no. 4, pp. 746–754, 2014.

[64] J. Nonnekes, N. Benda, H. Van Duijnhoven, F. Lem, N. Keijsers, J. W. K. Louwerens, A. Pieterse, B. Renzenbrink, V. Weerdesteyn, J. Buurke, and A. C. Geurts, "Management of gait impairments in chronic unilateral upper motor neuron lesions a review," JAMA Neurology, vol. 75, no. 6, pp. 751–758, 2018.

[65] J. W. Ramsay, M. A. Wessel, T. S. Buchanan, and J. S. Higginson, "Post-stroke muscle architectural parameters of the tibialis anterior and the potential implications for rehabilitation of foot drop," Stroke Research and Treatment, vol. 2014, 2014.

[66] M. E. Wiley and D. L. Damiano, "Lower-extremity strength profiles in spastic cerebral palsy," Developmental Medicine & Child Neurology, vol. 40, no. 2, pp. 100–107, 1998.

[67] B. A. Knarr, D. S. Reisman, S. A. Binder-Macleod, and J. S. Higginson, "Changes in predicted muscle coordination with subject-specific muscle parameters for individuals after stroke," Stroke Research and Treatment, vol. 2014, 2014.

[68] K. H. Cho, H. J. Lee, and W. H. Lee, "Intra-and inter-rater reliabilities of measurement of ultrasound imaging for muscle thickness and pennation angle of tibialis anterior muscle in stroke patients," Topics in Stroke Rehabilitation, vol. 24, no. 5, pp. 368–373, 2017.

[69] B. A. Knarr, J. Ramsay, T. S. Buchanan, S. A. Binder-macleod, and J. S. Higginson, "Quantification of atrophy and activation failure in the plantarflexors post- stroke," Stroke Research and Treatment, no. January 2015, pp. 5–7, 2015.

[70] J. W. Ramsay, T. S. Buchanan, and J. S. Higginson, "Differences in Plantar Flexor Fascicle Length and Pennation Angle between Healthy and Poststroke Individuals and Implications for Poststroke Plantar Flexor Force Contributions," Stroke Research and Treatment, vol. 2014, 2014.

[71] E. M. Halar, W. C. Stolov, B. Venkatesh, F. V. Brozovich, and J. D. Harley, "Gastrocnemius muscle belly and tendon length in stroke patients and able-bodied persons.," Archives of physical medicine and rehabilitation, vol. 59, pp. 476–484, oct 1978.

[72] H. Zhao, Y. Ren, Y.-n. Wu, S. Q. Liu, and L.-q. Zhang, "Ultrasonic evaluations of Achilles tendon mechanical properties poststroke," Journal of applied physiology, vol. 60611, pp. 843–849, 2009.

Appendices

Appendix A - Objective

In SCONE, the Objective describes the goal task for which you wish to optimize, through a weighted combination of Measures. The first unimpaired gait simulation, generated with the SCONE Tutorial [26], took long steps, showed abnormal ankle joint angles, with high and rapid plantarflexion and two double bumps in dorsiflexion, and an initial peak of vertical GRF (Fig. 1). To solve these issues and reduce the dynamics towards normal experimental values, 4 additional measures (Fig. 2) were introduced in the objective function:

- To prevent the abnormal initial high peak in the vertical GRF, a maximum value was set to 1.5 times body weight.
- To prevent abnormal high-speed plantarflexion at loading response and the two double bumps in dorsiflexion, the ankle angular velocity was restricted between -458 degrees/s (plantarflexion) and +401 degrees/s (dorsiflexion).
- To prevent abnormal long steps, the ROM of the hip was restricted between -15 degrees and 40 degrees, the stride duration between 0.2 s and 0.5 seconds and the stride length between 0.8 and 1.3 meters.

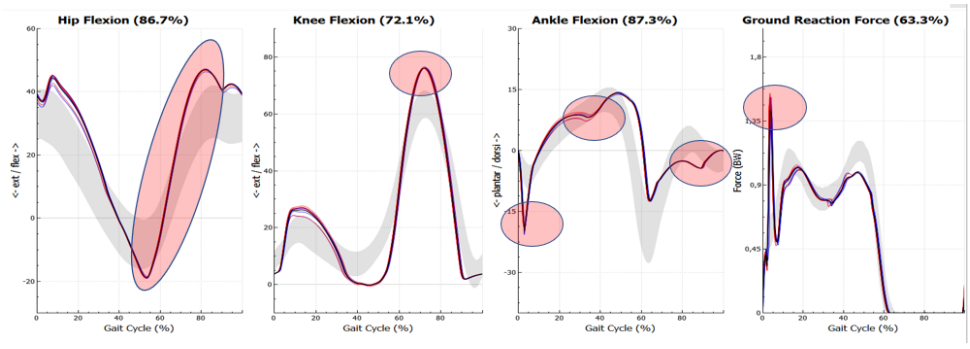

Figure 1: Hip, knee and ankle angles, in degree, and vertical ground reaction force (normalized per body weight) over the gait cycle during the gait simulation from the SCONE Tutorial, without our additional measures. Grey areas are experimental values from healthy subjects. The model took long steps, with high leg speed during swing (first graph on the left) and high knee flexion (second graph). The ankle trajectory was characterized by rapid plantarfexion at loading response and two double bumps in dorsiflexion in stance and swing (third graph) and there was a high GRF peak at loading response (fourth graph).

Other adjustments that improved or could have improved the simulation:

- Improvement of the muscle model, with Millard force-length curves, more realistic than previously used in the Thelen muscle model, remove unused parameters, used a set of initial parameters provided by Thomas Geijtenbeek.
- Add two more muscles in the model (Rectus Femoris and Biceps Femoris Short Head), however this solution required extra controllers, higher model complexity, and additional computational time and therefore was not implemented.

- Add a constant activation to all leg muscles, to increase stiffness around all the joints and prevent rapid joint displacements. However, the model kinematics did not reduce towards normal values (Fig. 3), therefore this solution was not implemented.

```
1  CompositeMeasure {
2    GaitMeasure { # Measure for gait, minimum speed = 0.5 m/s
3      name = Gait
4      weight = 10
5      threshold = 0.05
6      termination_height = 0.85
7      min_velocity = 0.5
8    }
9    EffortMeasure {   # Minimize cost of transport
10     name = Effort
11     weight = 0.1
12     measure_type = Wang2012
13     use_cost_of_transport = 1
14   }
15   CompositeMeasure {
16     name = DofLimits
17     symmetric = 1
18     DofMeasure {
19       weight = 0.1
20       dof = ankle_angle
21       position { min = -60 max = 60 squared_penalty = 1 } # deg
22       velocity { min = -458 max = 401 squared_penalty = 1 } # deg/s
23     }
24     DofMeasure {  # Prevent knee hyperextension
25       weight = 0.1
26       threshold = 5
27       dof = knee_angle
28       force { min = 0 max = 0 abs_penalty = 1 }
29     }
30     DofMeasure {# Restrict hip displacement to prevent too long steps
31       weight = 1
32       dof = hip_flexion
33       position { min = -15 max = 40 abs_penalty = 1 } # deg
34     }
35   }
36   StepMeasure {   # Restrict stride duration and length
37     name = StepLength
38     weight = 0.1
39     stride_duration { min = 0.2 max = 0.5 abs_penalty = 1 } # s
40     stride_length { min = 0.8 max = 1.3 abs_penalty = 1 } # m
41   }
42   ReactionForceMeasure {  # Penalty on the max. value of vertical GRF
43     name = GRF
44     start_time = 1
45     weight = 1
46     max = 1.5 # of body weight
47     abs_penalty = 1
48   }
49 }
```

Figure 2: Script of the SCONE Objective, with our additional measures in blue: restriction of ankle angular velocity (line 22), restriction of hip position (lines 30-35), stride duration and length (lines 36-41), penalty on the maximum value of the vertical ground reaction force (lines 42-48).

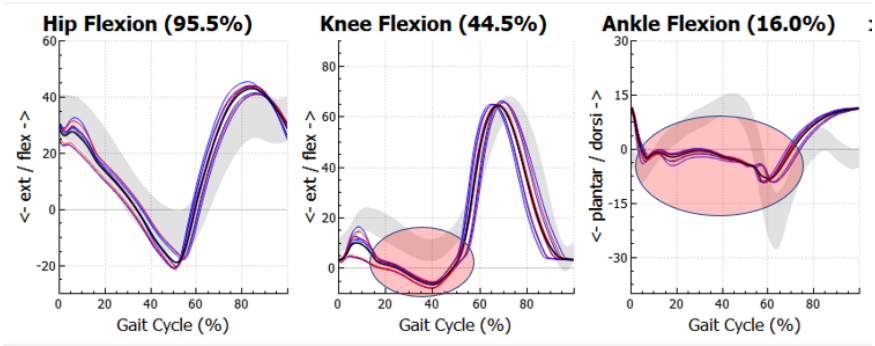

(a) Minimum activation = 0.05. The model shows knee hyperextension and insufficient ankle dorsiflexion in stance.

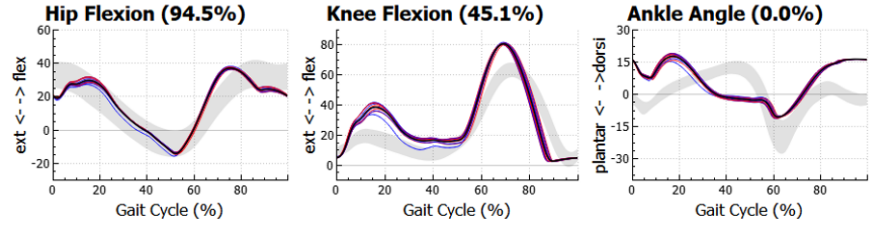

(b) Minimum activation = 0.01. The model shows insufficient hip flexion at landing and foot strike, high knee flexion in stance and ankle kinematics are completely off.

Figure 3: Hip, knee and ankle angles in degree over the gait cycle during the gait simulation with increased minimum activation, of all leg muscles, compared with experimental values from healthy subjects (grey areas).

Appendix B - List of NMS alterations and deficits

Table 1: Overview of structural muscular and neural alterations of the neuromusculoskeletal model and the corresponding deficits occurring in stroke and Cerebral Palsy patients.

Muscle	NMS model alterations	Deficits in patients	Ref
Tibialis Anterior	Min. control	Increased background level of contraction in spastic muscle	[43]
	Min. activation		
	Max. control	Dorsiflexor muscle activation failure after stroke	[52, 65]
	Max. isometric force	Dorsiflexor muscle weakness after stroke and CP	[31–34, 41, 66, 67]
	Optimal fiber length	No significant difference after stroke	[65]
	Tendon slack length	Not clear if properties of TA tendon change after stroke	[65]
	Tendon force length curve		
	Pennation angle at optimal fiber length	Smaller pennation angle paretic side stroke patients No significant difference after stroke	[68] [65]
Gastrocnemius	Min. control	Overactivity of Gastrocnemius in stroke and CP patients	[44, 45]
	Min. activation		
	Max. control	Plantarflexor muscle activation failure after stroke	[52, 69]
	Max. isometric force	Plantarflexor weakness after stroke	[52, 69, 70]
	Optimal fiber length	Gastrocnemius lengths shorter in hemiplegic muscles post stroke	[37, 71]
	Pennation angle at optimal fiber length	No differences after stroke	[70]
	Tendon slack length	Increased tendon length post stroke No change in tendon length after stroke	[37] [71]
	Tendon force length curve	Decreased tendon stiffness after stroke	[71, 72]
	Passive force length curve	Increased fascicular stiffness after stroke	[37, 52]
Soleus	Min. control	Overactivity of Soleus in stroke and CP patients	[44, 45]
	Min. activation		
	Max. control	Plantarflexor muscle activation failure after stroke	[52, 65]
	Max. isometric force	Plantarflexor weakness after stroke	[52, 69, 70]
	Optimal fiber length	Soleus lengths shorter in hemiplegic muscles post stroke	[37]
	Pennation angle at optimal fiber length	No differences after stroke	[70]
	Tendon slack length	Increased tendon length post stroke	[72]
	Tendon force length curve	Decreased tendon stiffness post stroke	[37, 72]
	Passive force length curve	Increased fascicular stiffness after stroke	[37, 52]

Appendix C - AFO model

To determine the parameters of the AFO model we performed repeated varied attempts. Here we provide our successes and failures to assist other researchers in future studies focusing on the development of the AFO model. First, we looked at different functions available in OpenSim:

- Coordinate Limit Force at the ankle joint: applies a force to limit the range of motion of the ankle. Once you set (multiple) upper and lower limits of the coordinate value, it applies linear stiffness, from K_{upper} to K_{lower}. The AFO should not apply a linear, but an exponential force. One way to solve this problem is to define multiple ranges, each with a linear stiffness depending on the steepness of the exponential curve (Fig. 4). However, discontinuities in the derivative at the connections of the linear domains may affect the optimization.

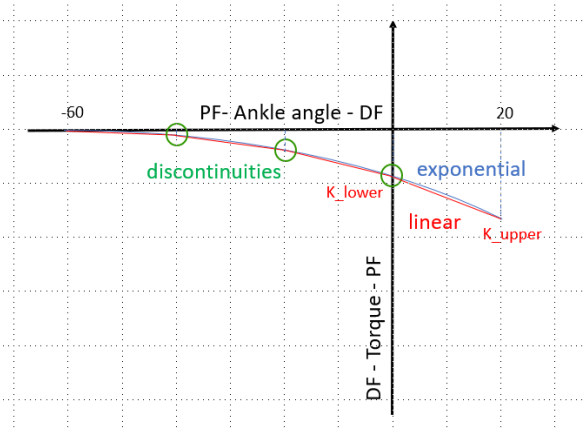

Figure 4: The Coordinate Limit Force applies linear stiffness when the ankle angle is between an upper and lower limit. The exponential torque is approximated with linear torque, setting multiple limits, but discontinuities may affect the optimization.

- Prescribed Force Class: applies a force and/or torque to a body, as a function of time. We need to apply torque as a function of the ankle angle. Ankle angle is a function of time but will be also affected by the torque. Therefore, the torque can not be expressed as a function of time.
- Expression Based Point to Point Force: applies a force between two points, as a function of the distance between the two points. The resultant torque will depend on both the force and the moment arm.

We used the last approach and chose the two attachment points of the SOL muscle (Fig. 5) to simplify the calculation of the distance between the points and the moment arm. The distance between the two points is the SOL fiber length, and the moment arm is the SOL ankle moment arm, both calculated with OpenSim (Fig. 6).

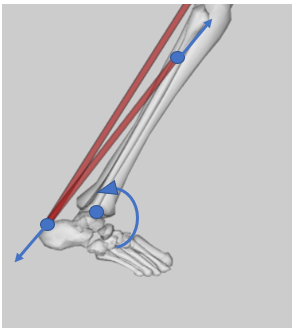

Figure 5: Force between the two attachment points of the SOL muscle generates a torque around the ankle joint. As the distance between the two points increases (dorsiflexion direction), the force increases exponentially.

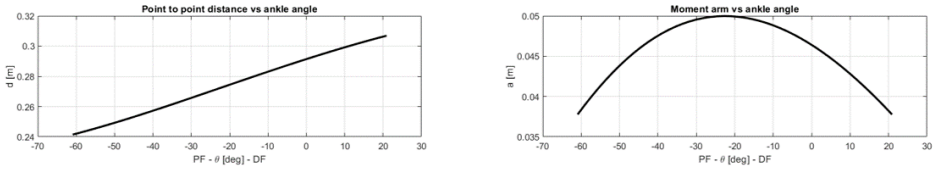

Figure 6: Left: distance between the two application points of the force, or SOL muscle length, vs the ankle angle. Right: moment arm of the AFO force, or SOL-ankle moment arm, vs the ankle angle.

We first tried parameters used for the first prototype (Eq. 1, Table 2, Fig. 7).

$$T_{PF}(\theta) = c_1 e^{c_2(\theta - c_3)} \rightarrow F(d) = ae^{bd} \tag{1}$$

However, the simulation did not even initiate ('waiting for first evaluation') because the force was too high due to the small moment arm.

Table 2: Parameters of the exponential functions of the modelled AFO and Point to Point Force based on the first prototype.

	c_1	c_2	c_3	a	b
AFO1	2.465	0.079	-14.045	0.2703	139.9
AFO2	3.429	0.094	-5.626	0.06054	166.5
AFO3	7.351	0.089	6.617	0.06443	157.6
AFO4	0.267	0.119	-18.183	0.002948	211.3
AFO5	5.566	0.113	11.237	0.003291	200.5
AFO6	3.953	0.089	10.910	0.002365	157.6

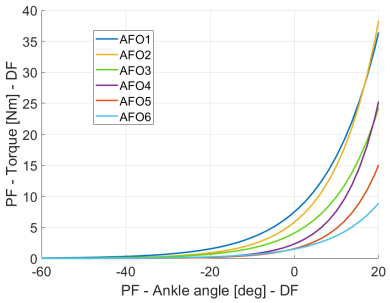

(a) Torque applied by the AFO around the ankle joint as a function of the ankle angle.

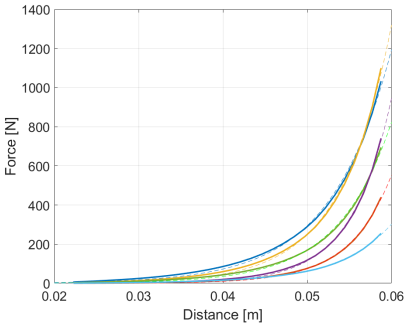

(b) Force applied by the AFO model, between the two attachment point of the SOL, as a function of the distance between the two points.

Figure 7: Characteristics of the AFO model based on the first prototype.

Next, we used a step wise approach: first retrieve ankle joint passive stiffness of the model, then choose a level of compensation, then apply the torque to compensate, and repeat for each alteration of passive muscle parameters.

- To retrieve passive stiffness of the modelled ankle joint, we multiplied the passive force of GAS and SOL muscles with their ankle moment arm: $T_{ankle} = F_{p,GAS} * arm_{GAS} + F_{p,SOL} * arm_{SOL}$.
- Theoretically, an external torque can fully compensate (100% compensation) the passive ankle joint stiffness. (In practice, this is limited by the construction of the mechanism, which needs to exert a high torque with a small moment arm.) We fitted an exponential function (fit(x,y,'exp1') in MATLAB) to $-T_{ankle}$ to obtain $T_{AFO}(\theta) = a_T e^{b_T \theta}$ and $F_{AFO}(d) = a_F e^{b_F d}$ (Table 3).

Table 3: Parameters of the exponential functions of the modelled AFO angle-dependent torque and corresponding distance-dependent force.

	a_T	b_T	a_F	b_F
-10% GAS l_0	-1.853	0.1081	0.007625	187.2
-30% GAS l_0	-17.13	0.06018	3.299	104.4
-50% GAS l_0	-79.79	0.03721	81.45	67.6

- The new passive stiffness is equal to $T_{ankle} + T_{AFO}$. This is closer to T_{ankle} of the unimpaired model (Fig. 8a), except with higher passive stiffness, as it also happens experimentally.
- Each change in passive muscle parameter results in a new ankle stiffness. Theoretically, when combining parameters, we would need more compensation

than with isolated changes. When we reduce muscle force, increase minimum activation of the muscles or add a reflex, however, there is no way to directly calculate the increased stiffness of the ankle. In these conditions, the AFO would compensate a normal ankle stiffness and not an increased stiffness.

However, the force was still too high due to the small moment arm (Fig. 8b).

At the end, we applied lower forces, trying out several parameters: to quickly rule out those AFO configurations that did not give plausible results (the model fell immediately or made absurd movements, or the force was too high and the the simulation did not initiate) we first used SCONE 'evaluate scenario' It means that the same neural controls are used, without optimization. In this way, the solution was obtained immediately, without waiting for the computational time, but the solution was not optimal. Then, we optimized the scenario, using optimized neural controls based on the objective function performance.

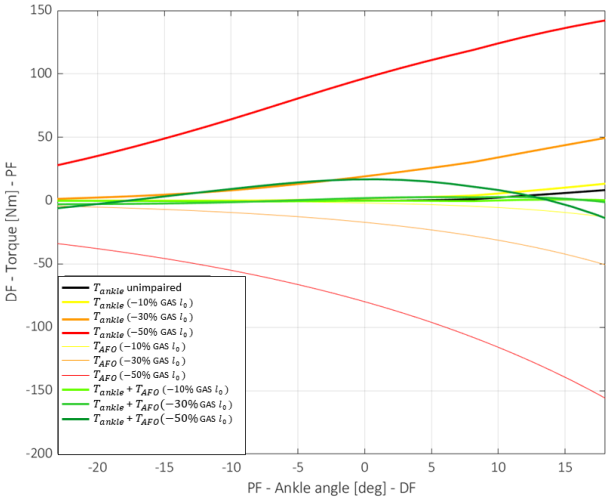

(a) Passive stiffness of the modelled ankle joint increases when changing the passive muscle parameters, i.e. Gastrocnemius optimal fiber length (yellow, orange, red thick lines). The AFO compensates for the increased stiffness by applying a torque around the ankle joint (yellow, orange, red thin lines). Stiffness of the total system, AFO+ankle, (green) is closer to the passive stiffness of the unimpaired model (black).

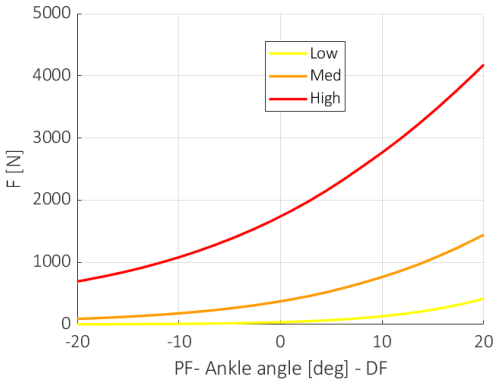

(b) Forces applied between the two attachment points of the SOL, that generate the above AFO torques around the ankle joint.

Figure 8: Characteristics of the AFO model based on passive stiffness compensation.